48
8-15-95 JS (2)

PREPARED FOR THE U.S. DEPARTMENT OF ENERGY,
UNDER CONTRACT DE-AC02-76-CHO-3073

PPPL-3112
UC-420,426

PPPL-3112

SIMULATIONS OF ALPHA PARAMETERS IN A TFTR SUPERSHOT WITH HIGH FUSION POWER

BY

R.V. BUDNY, M.G. BELL, A.C. JANOS, ET AL.

JULY 1995

PPPL PRINCETON PLASMA PHYSICS LABORATORY

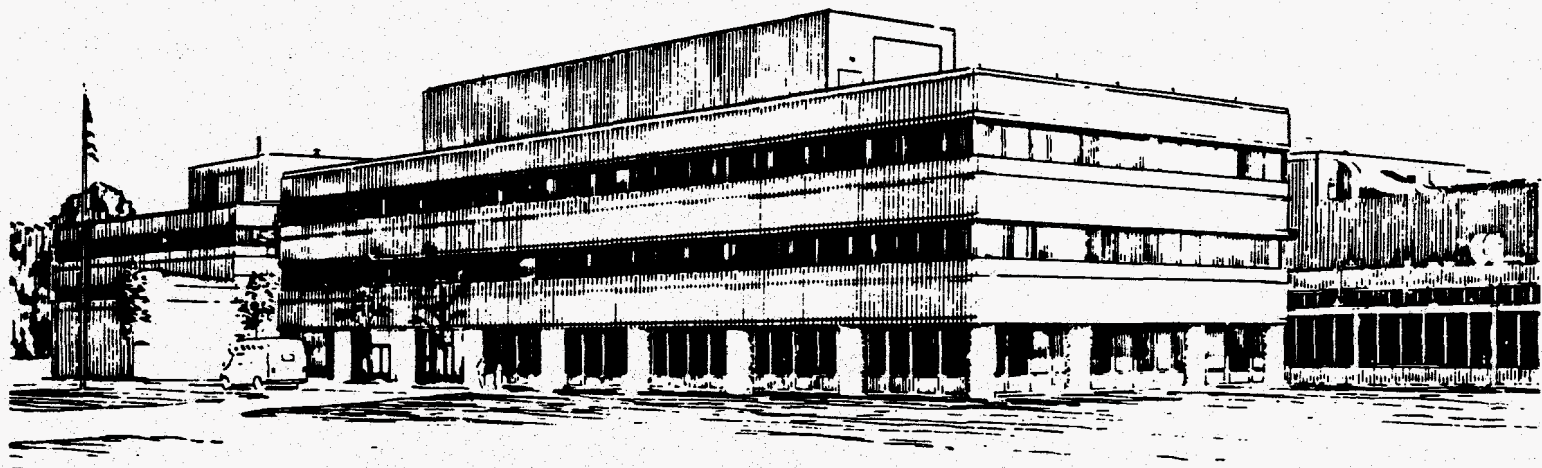

PRINCETON UNIVERSITY, PRINCETON, NEW JERSEY

NOTICE

NOTICE

Simulations of Alpha Parameters in a TFTR DT Supershot with High Fusion Power

R.V. Budny, M.G. Bell, A.C. Janos, D.L. Jassby,
L.C. Johnson, D. Mansfield, D.C. McCune, M.H. Redi, J.F. Schivell,
G. Taylor, T.B. Terpstra, M.C. Zarnstorff, and S. J. Zweben

Princeton University
Plasma Physics Laboratory
P. O. Box 451, Princeton NJ, 08544

May 30, 1995

Abstract

A TFTR supershot with a plasma current of 2.5 MA, neutral beam heating power of 33.7 MW, and a peak DT fusion power of 7.5 MW is studied using the TRANSP plasma analysis code. Simulations of alpha parameters such as the alpha heating, pressure, and distributions in energy and $v_{parallel}$ / v are given. The effects of toroidal ripple and mixing of the fast alpha particles during the sawteeth observed after the neutral beam injection phase are modeled. The distributions of alpha particles on the outer midplane are peaked near forward and backward $v_{parallel}$ / v. Ripple losses deplete the distributions in the vicinity of $v_{parallel} / v \approx -0.4$. Sawtooth mixing of fast alpha particles is computed to reduce their central density and broaden their width in energy.

1. Introduction

Experiments with deuterium-tritium (DT) plasmas were started in TFTR during 1993 [1,2,3]. Several experiments have been dedicated to maximizing the fusion power. In November 1994, DT discharges with neutral beam injection (NBI) heating of 39 MW, plasma currents of 2.7 MA, and toroidal fields of 5.6 T achieved fusion power at peak rates up to 10.7 MW and at peak power densities above 2.5 MW/m^3.

The previous record was set in May 1994, when DT discharges with NBI heating of 34 MW, plasma currents of 2.5 MA, and toroidal fields of 5.1 T achieved fusion power at peak rates up to 9.2 MW [4]. The discharge with the highest peak rate disrupted, but similar discharges with peak rates up to 7.5 MW did not disrupt and had sustained high fusion power production for approximately 0.5 sec. Analysis of the highest non-disruptive discharge from May 1994 with a peak rate of 7.5 MW is discussed in this paper.

This discharge has been extensively modeled using the TRANSP time-dependent plasma analysis code [5-8]. The modeling provides calculations of profiles of the D and T densities, the hydrogenic isotopic mass, the fusion reactions, fast ion parameters, and the alpha heating. Results are in approximate agreement (~ 1σ) with available measurements [5].

A detailed prediction for a DT supershot based on a moderate-performance, reproducible D-only supershot was described before the DT campaign [7]. That simulation predicted 5.6 MW of fusion power with a fusion power ratio $Q_{DT} \equiv P_{DT} / P_{NB} = 0.23$. This paper updates those simulations using an actual high-performance DT discharge. One of the predictions [7] made before the DT campaign was that the stored energy in DT-NBI supershots would be about 10% higher than in D-only supershots. This predicted increase is due to changes in the NBI parameters, the effects of alpha-electron heating, and the additional stored energy of the alphas. The observed increase is twice as large [1]. The extra increase is attributed to an intrinsic isotopic scaling of the thermal plasma confinement with isotopic mass [8,9].

Several methods are being used to measure facets of the confined alpha particle distributions in TFTR plasmas. One method uses charge exchange recombination spectroscopy of alphas excited by NBI ions [10]. Another method analyses the energy of neutral alpha particles from double charge exchange in pellet ablation clouds [11]. A third method is designed to analyze gyrotron Thomson scattering from alpha particles

[12]. These diagnostics measure the alpha energy in different regions of energy and $\lambda \equiv v_{parallel} / v \equiv \cos(\text{pitch angle})$. This paper gives simulations for the alpha distributions in energy and λ.

Supershots generally exhibit sawteeth before and after the NBI phase. These sawteeth are accompanied by significant decreases in the central plasma parameters such as T_e and n_e. If the fast ions are mixed during the sawteeth crashes, then the central neutron emission and alpha parameters would be affected. Fast ion mixing is modeled in TRANSP and simulations of this mixing are being used to test empirically whether such mixing occurs.

General plasma conditions for the discharge are discussed in Section 2. The TRANSP modeling typically used for TFTR discharges is discussed in Section 3. Alpha particle parameters are discussed in Section 4. The fast alpha distributions are discussed in Section 5.

2. Plasma Conditions for 76770

The neutral beams injected 19.6 MW of T and 14.1 MW of D from 3.5 to 4.3 sec. Plasma conditions at the time of peak neutron emission rate ($\approx$ 4.0 sec) are $I_p = 2.5$ MA, $B_{TF} = 5.1$ T, $R_0 = 2.5$ m, $a = 0.9$ m, and $q_\psi(a) = 4$. The q_ψ profile was not measured, but $q_\psi(0) \approx 0.8$ is typically measured in similar discharges. The total energy confinement time is 0.22 sec. This relatively high confinement time resulted from intensive Li pellet injection [13] into the ohmic phases of discharges during this experimental run in order to condition the vessel walls.

Supershots generally exhibit sawteeth during their ohmic phases, and occasionally during the neutral beam phase. Typical behavior with high NBI power is that the pre-NBI sawteeth disappear after one or two crashes during the start of the NBI. After $\approx$ 0.1 sec, sawteeth are generally not observed during the NBI except if the NBI power is low (< 25 MW) and the plasma current I_p is high (> 2 MA). They start about $\approx$ 0.2 sec after the termination of NBI with regularity. Examples of the effects of sawteeth and the Li pellet for 76770 are seen in the $T_e(0)$ trace in Fig. 1. Empirical evidence for degree to which the beam ions and fusion alpha ions are mixed during sawteeth crashes is not fully established. This mixing is computed to have significant consequences on the energy and pitch angle distributions of the fast ions.

There is little direct evidence for alpha particle effects on the plasma in supershots. One indirect piece of evidence is that the measured alpha losses are normal in supershots that do not have excessive MHD activity [14]. The measured rates of fast alpha particles collected in detectors at poloidal angles 20^0 [15] and 90^0 below the midplane for 76770, normalized to the total neutron emission rate are approximately constant in time.

3. TRANSP Modeling Capabilities

The TRANSP plasma analysis code is used to model the time evolutions of plasma parameters. The energy, particle, and magnetic field dynamics are computed. Measured plasma profiles and the location of the last closed flux surface are specified. Three temperatures (T_e, hydrogenic ion T_i, and impurity ion T_x) are modeled. Typically, measurements of the electron temperature (from ECE) and of the temperature and toroidal rotation velocity of the trace carbon impurity (from neutral-beam induced charge-exchange recombination spectroscopy) are used as initial inputs. The hydrogenic temperature T_i is computed from the measured T_x in TRANSP [6]. This computed central T_i is lower than T_x by several keV. The difference is largest during the first ~0.2 sec of the NBI.

Up to five thermal ion species and one impurity species can be modeled simultaneously in TRANSP. For the modeling described here, the thermal species are H, D, T, He^4, Li, and one heavier impurity. The hydrogen and impurity species are non-negligible components, as discussed in Ref. [5]. The lithium has small relative concentrations during the NBI phase. The helium ash is estimated to have small relative concentrations (peaking at n_e / 1000 in the center).

The equilibrium flux surfaces are calculated by solving the fixed-boundary Grad-Shafranov equations using the total (beam + thermal) pressure. Typically ~ six seconds of the discharge evolution are modeled, starting within 0.5 sec of the discharge initiation and continuing through the neutral beam injection. Modeling the early phase allows a more accurate computation of the magnetic field diffusion and the q_ψ profile.

Fast Ions - Monte-Carlo techniques [16] are used to compute the deposition of the neutral beams, and the distributions of the beam ion and fusion ions. The beam ions and fusion products are assumed to slow down either classically or with an added anomalous radial diffusivity. The assumptions of classical slowing down and loss have

been checked in the case of beam ions [17] and DD fusion products [18]. For instance, if a constant radial diffusivity of ~ 0.05 m^2/sec is assumed to be superimposed on the classical slowing down of the beam ions, then the TRANSP results for the total neutron rates and the stored energies would differ significantly from the measurements [17]. We extrapolate these results by assuming no anomalous diffusion for the fast alpha particles. The losses of beam ions and alpha particles on orbits that intercept the limiter or wall are computed in TRANSP.

The TRANSP modeling is tested and confirmed by comparing simulations with measurements. Examples of comparisons are the Shafranov shifts, the stored energy, and the neutron emission profile. These tests are interrelated and provide global checks of the modeling. For instance, the Shafranov shifts, which depend on the total pressure, effect the plasma profiles that are used to calculate the plasma and beam pressure. Comparisons are discussed in detail in Ref. [5].

Neutron emission - The measured and simulated total neutron emission rates are shown in Fig. 2-a. The absolute measurement uncertainty is $1\sigma \approx 7\%$. These are in good agreement for the first 0.6 sec of NBI. Later the simulated total is systematically higher than the measured value. The neutron emission chordal profiles are measured by a collimator array. The absolute measurement error is $1\sigma \approx \pm 15\%$. Time evolutions of the simulations and measurements are compared in Fig. 2-b. Profiles near the time of peak emission are compared in Fig. 2-c. The simulated profiles are shifted several cm outward with respect to the measured profiles. Accurate simulations of the central neutron emission rates are desired since the alpha parameters depend sensitively on the central fusion rate. The simulation depends sensitively on the Z_{eff} of the plasma, which is not known accurately for reasons discussed in Ref. [5].

Fusion Power - The peak neutron emission rate is $S_n = 2.7 \times 10^{18}$/sec, so the fusion yield, P_{DT} ($\equiv S_n / 3.6 \times 10^{17}$ [MW/sec]) is 7.5 MW. The calculated fraction of the total from thermonuclear reactions is 25%. The central fusion power density is dominantly thermonuclear, as shown in Fig. 3. The central alpha-electron heating rate is shown for comparison. Its peak occurs after the peak fusion rate. This is discussed in more detail in Section 4.

Ripple - A model for estimating toroidal field ripple effects of fast ions has been included in TRANSP [19,20]. The magnitude of the toroidal field ripple is input along with a threshold set as a factor times the Goldston-White-Boozer [21] stochastic ripple threshold. When the turning points of fast ion orbits are in locations where the toroidal field ripple is above this threshold, the ions are ejected from the plasma. The choice of

the multiplier has been adjusted by comparisons of TRANSP and guiding center code calculated losses.

Sawteeth - The occurrence of sawteeth in TFTR supershots is consistent with a criterion of drift frequency, ω_*-stabilization of the collisionless m = 1 reconnection mode [22,23]. Sawteeth may have important implications for alpha parameters due to mixing. TRANSP uses a phenomenological sawtooth model which is invoked at the observed sawtooth crash times if $q_\psi(0)$ is less than 1. The magnetic flux surfaces are shifted using the Kadomtsev helical flux mixing model [24]. The calculated mixing radius is ≈ 30% larger than the calculated $q_\psi = 1$ radius.

The amount of current mixing can be adjusted in TRANSP to less than the full current mixing in the standard Kadomtsev model. A weighted average of the unmixed and fully mixed current profiles is imposed after the crash. For the results given here the weighting is 70% of the unmixed and 30% of the fully mixed current. These ranges predict $q_\psi(0)$ values in approximate agreement with observations. Full (100%) current mixing predicts $q_\psi(0)$ values which increase after the sawteeth crashes to values that are too high (close to one) for consistency with measurements [25]. The sawtooth prescription in TRANSP generally calculates the (m,n) = (1,1), (4,3), and (3,2) surfaces which are within ~ 5 cm of the locations of sawteeth inversions and of coherent (4,3) and (3,2) MHD activity indicated by fast T_e measurements.

TRANSP can be run either with or without fast ion mixing. In the case where the fast ions are assumed to mix, the ions are shifted with the flux surfaces conserving helical flux. The poloidal angle for each Monte Carlo ion is randomized and the values of $v_{parallel}$ and $\mu \equiv v_{perp}^2 / B$ are conserved through the crash. This prescription alters the energies and $\lambda \equiv v_{parallel} / v$ of the fast ions and converts some of the passing ions to trapped and vice versa.

4. Alpha Parameters

The alpha slowing down and pitch angle scattering are modeled. The slowing down and pitch angle scattering times are considerable longer than the corresponding times for beam ions, as shown in Figs. 4. The confined alphas are calculated to mainly heat electrons. The alpha-electron heating is predicted to be a significant portion of the total election heating in the center. Its profile is compared with the beam-electron and thermal ion-electron heating in Fig. 5.

The calculated time evolutions of the central fast alpha particle density n_α, average energy $<E_\alpha>$, toroidal beta β_α, and electron heating power are shown in Figs. 6. During the NBI phase $n_\alpha(0)$ increases steadily, while $<E_\alpha(0)>$ decreases. These contrary trends cause $\beta_\alpha(0)$ to peak during the NBI. Results are given with and without fast ion mixing. If the fast ions are assumed to mix during the sawtooth crash with the prescription described in the previous section, these central parameters decrease precipitously after the crash. If the ions are not mixed by sawteeth, these central parameters tend to decrease gradually after the termination of NBI. In this case, the alpha heating peaks during the sawteeth crashes and during the pellet (due to the rapid thermalization in the high density pellet cloud).

The fast ion mixing prescription described above has dramatic effects on the fast ion profile, as shown in Fig. 7. The independent variable is the square root of the normalized toroidal flux, x. This variable is close in value to the normalized minor radius, r/a.

The ripple model predicts effects on alpha parameters that are more subtle than the sawtooth mixing. Profiles are shown in Figs. 8. The ripple losses of energy for the alphas, D-beam ions, and T-beam ions are 9%, 11%, and 13%, respectively. The particle losses are about 1% higher. The first-orbit losses are relatively small ($\approx$ 3%) since the plasma current is relatively high (2.5MA).

5 - Alpha Distributions

Monte Carlo methods are used to track orbits of individual fast ions. The parameters for these are sampled to generate their distribution in the laboratory rest frame,

$$f_j(E_j,\lambda_j,x,t) \equiv \frac{dn_j}{dV dE_j d\lambda_j}$$

The independent variables are the energy E_j of the fast species j, $\lambda_j \equiv v_{parallel} / v \equiv$ cos(pitch angle) with $v_{parallel}$ the component of v in the direction of the plasma current, and the location in space and time. These are normalized so that their integral over E_j and average over λ_j gives the fast ion spatial density. An example of the flux-surface average is shown in Fig. 8-a.

These distributions are formed by censusing the fast ions passing through zones in a 2 dimensional slice at fixed toroidal angle. For the results given here, 100 equal energy intervals and 50 equal λ intervals are used. The zones are chosen to lie along the outer midplane. The radial spacing of the zones are equal intervals of x. The poloidal widths of the zones are indicated in Fig. 9. The distributions are not the same as the orbit averages for the fast ions.

The results given here are from TRANSP runs using 8000 Monte Carlo D and T beam ions, and 8000 fusion alpha ions. The results are averaged over 80 msec at various times during the discharge. These times are selected throughout the NBI phase, before and after the post-NBI sawteeth, and before the post-NBI pellet. The sampling windows are shown in Fig. 1.

The results for the beam ion distributions, f_D and f_T, and for f_α are qualitatively similar to the results given in Ref. [7]. More detailed results for f_α are given here. First we show the effects of ripple by comparing f_α before the first post-NBI sawtooth. The plots in Figs. 10 compare $f_\alpha(E_\alpha,\lambda,x=0.5,t=4.43s)$ calculated with and without the ripple model. The results for both cases show a peaking at positive λ. This is due to non-zero orbit effects and the λ peaking of the beam ions. The alpha distributions have regions with relatively low values near $\lambda \approx -0.4$ and $E_\alpha \approx 2.5$ MeV. This is a consequence of the trapped ions with negative λ on the midplane having banana orbits with x increasing away from the midplane, whereas those with positive λ have banana orbits with x decreasing away from the midplane. Some of the orbits with increasing x leave the last closed flux surface and can get scraped off. Also the slowing down time decreases with x, as shown in Fig. 4-a, so the ions with negative λ slow down more rapidly. In the case where the ripple model in turned on (Fig. 10-b), this depletion is more pronounced since the ripple loss is more likely at larger x. These effects are seen to a lesser extent in the center ($x \approx 0$), and to a larger extent at $x > 0.5$. At $x \approx 0.7$ these effects are very pronounced, as shown in Figs. 11.

The effects of fast-ion sawooth mixing can be seen in the distributions after the sawtooth crashes. Effects on the energy distribution are shown in Fig. 12. The results are averaged from 4.52 to 4.53 sec and for $-0.1 < \lambda < +0.1$. The mixing has the effect of depleting the distribution at x=0 and increasing it at x=0.5. The mixing and ripple effects on the pitch angle distribution at x=0.5 are shown in Figs. 13. Their combined effects cause a trough near $\lambda \approx -0.2$.

Thermal Doppler broadening in E_α of f_α is not yet included in TRANSP; however, the broadening due to the alphas slowing down and scattering is included. The

broadening in the center (x=0) is shown in Figs. 14. During the first 0.5 sec of NBI the distribution is inverted. Later it develops into a slowing down distribution. Both ripple and sawtooth mixing effects are included in this result.

6 - Summary

TRANSP simulations of alpha parameters are given for a high performance, non-disruptive TFTR DT-NBI supershot with a peak fusion power of 7.5 MW. Effects of ripple loss and sawteeth are modeled. Trapped fast ions are assumed to be ejected from the plasma if their turning points are above a preset factor times the Goldston-White-Boozer threshold. The ripple losses of alpha particles are estimated to be ≈ 10% for the plasma discussed in this paper. The sawtooth model in TRANSP for the thermal plasma is a modification of the Kadomtsev flux and current mixing model. In TFTR discharges, the amount of current mixing that gives q_ψ profiles in approximate agreement with measurements is about 30%. A model for fast ion mixing during the sawtooth crashes is also incorporated in TRANSP. Their guiding centers are assumed to remain on the flux surfaces, and their parallel velocity is assumed to be conserved. Results with and without fast ion mixing during the post-NBI sawteeth are compared. The central alpha density and pressure are predicted to decrease significantly if the fast ions mix during sawtooth.

Monte Carlo methods are used to calculate fast ion distributions. Results are given for the distributions on the outer midplane versus energy and λ = cos(pitch angle). The central beam ion distributions in λ are peaked near forward and backward pitch angles. Ripple losses deplete regions with $\lambda \approx -0.2$ and E ≈ 2.5 MeV. Sawtooth mixing of the fast alpha particles is predicted to alter the pitch angle distributions.

Acknowledgments

We wish to thank J. D. Strachan for encouragement and the U. S. Department of Energy for support under the Contract No. DE-AC02-76-CHO-3073.

References

[1] R. J. Hawryluk, H. Adler, P. Alling, *et al.*, Phys. Rev. Lett. **72** (1994) 3530.

[2] J. D. Strachan, H. Adler, P. Alling, *et al.*, Phys. Rev. Lett. **72** (1994) 3526.

[3] J. D. Strachan, H. Adler, P. Alling, *et al.*, Plasma Physics and Controlled Fusion **12** (1994) 33.

[4] M. G. Bell, C. W. Barnes, R. V. Budny, *et al.*, IAEA (A-2-I-2).

[5] R. V. Budny, M. G. Bell, R.E. Bell, et *al.*, PPPL-3039.

[6] R. V. Budny, M. G. Bell, H. Biglari, *et al.*, Nucl. Fusion **32** (1992) 429.

[7] R. V. Budny, Nucl. Fusion **34** (1994)-1247.

[8] R. V. Budny, M. G. Bell, D. K. Mansfield, J.D. Strachan, *et al.*, proceedings of the 21 th EPS, Montpellier, (1994) **18B-I**, 82.

[9] S.D. Scott, *et al.*, Phys of Fluids.

[10] G. R. McKay, R. J. Fonck, T. A. Thorson and B. C. Stratton, "Implementation of alpha CHERS diagnostic for DT operation in TFTR", to be published in Rev. of Scientific Instruments; G. R. McKay, *et al.*, submitted to Phys. Rev. Letters.

[11] R. Fisher, J.M. McChesney, A.W. Howold, *et al.*, Rev. of Scientific Instruments **63** (1992), 4499. M. Petrov, R. Budny, *et al.*, submitted to Nucl. Fusion (this workshop).

[12] J. Machuzak, P. P. Woskov, J. Gilmore, *et al.*, "TFTR 60 GHz Alpha Particle Collective Thomson Scattering Diagnostic," to be published in Rev. of Scientific Instruments.

[13] J. A. Snipes, E. S. Marmar, J. L. Terry, *et al.*, Journal. of Nucl. Materials **196-198** (1992) 686.

[14] S.J. Zweben, *et al.*, "Alpha Particle Loss in TFTR DT experiments", submitted to Nucl. Fusion.

[15] S.J. Zweben, *et al.*, submitted to Nucl. Fusion (this workshop).

[16] R. J. Goldston, D. C. McCune, H. H. Towner, *et al.*, Journal Comp. Physics, **43** (1981) 61.

[17] E. Ruskov, W. Hedibrink, and R.V. Budny, to be published in Nuclear Fusion.

[18] J.D. Strachan, C.W. Barnes, R.V. Budny, *et al.*, to be published in Nuclear Fusion.

[19] M. H. Redi, M. C. Zarnstorff, *et al.*, to be published in Nucl. Fusion.

[20] M. H. Redi, R.V. Budny, *et al.*, submitted in Nucl. Fusion (this workshop).

[21] R. J. Goldston, R. B. White, and A. H. Boozer, Phys. Rev. Lett. **47** (1981) 647.

[22] F.M. Levinton, L. Zakharov, S.H. Batha, *et al.*, Phys. Review Letters, **72** (1994) 2895.

[23] L. Zakharov, F. Levinton, S. Migliuolo and B. Rogers, "The Theory of Stabilization of Sawtooth Oscillations in TFTR Supershots", PPPL report 2953 (1994).

[24] B. B. Kadomtsev, Sov. J. Plasma Phys. **1** (1975) 389.

[25] M. Yamada, F. M. Levinton, N. Pomphrey, *et al.*, Phys. Plasmas **1** (1994) 3269.

Figure Captions

Fig. 1 Evolutions of the central electron temperature measured from electron cyclotron emission. The sawteeth and pellet effects on $T_e(0)$ are indicated. The sampling windows used for averaging the Monte Carlo data used for the fast ion distributions are also indicated.

Fig. 2 Time evolutions of a) the measured and simulated total neutron emissivity and the simulated contributions from beam-thermal, beam-beam and thermonuclear fusion reactions; b) comparisons of the measured and simulated chordal neutron emissivity; and c) profiles near the time of peak neutron emission.

Fig. 3 Time evolutions of the central fusion power densities of the total DT reactions, of the thermonuclear reactions, and of the alpha-electron heating.

Fig. 4 Profiles of the a) slowing down times, and b) pitch angle scattering times of the alpha particles and beam ions at birth.

Fig. 5 Profiles versus major radius of the dominant electron heating terms showing significant central alpha-electron heating.

Fig. 6 Evolutions of central alpha parameters assuming a) fast ion sawtooth mixing, and b) no fast ion sawtooth mixing. The differences in the time evolutions before the post-NBI sawtooth are due primarily to Monte Carlo fluctuations.

Fig. 7 Profiles a) the fast alpha density and b) q_ψ after the first post-NBI sawtooth. The independent variable is the square-root of the normalized toroidal flux (approximately r/a). The effect of sawtooth mixing on the alphas is shown. With the mixing prescription generally used for modeling TFTR discharges, the effect on q_ψ is negligible.

Fig. 8 Profiles of the a) fast ion density, and b) β_α near the end of the NBI phase. The effects of ripple loss are indicated.

Fig. 9 Zones used for computing fast ion distributions. The radial intervals are determined by combining adjacent pairs of the 20 flux surfaces computed by TRANSP in solving for the MHD equilibrium. The poloidal angles are equally spaced within each flux surface and the number of poloidal angle increments increases as the flux increases. The zones for the sampling the distributions on the outer midplane are indicated. Pairs of poloidal zones, one below and one above the midplane are combined for the results presented here.

Fig. 10 Distribution of fast alphas in E and λ at the half-radius, just before the first post-NBI sawtooth crash. For a) the ripple model is assumed to be negligible. For b) the usual ripple model is used. The distributions are averaged in energy using a width of 0.1 MeV.

Fig. 11 Distribution of fast alphas in E and λ at x=0.7, just before the first post-NBI sawtooth crash. For a) the ripple model is assumed to be negligible. For b) the usual ripple model is used. The distributions are averaged in energy using a width of 0.1 MeV.

Fig. 12 Distribution of fast alphas in x with λ near 0.0, and E_α = 0.5 and 1.0 MW, just after the first post-NBI sawtooth crash. Two cases are compared: a) the fast-ion sawtooth mixing and the ripple losses are assumed to be negligible; and b) the usual fast ion mixing and ripple models are used.

Fig. 13 Distribution of fast alphas in λ at x = 0.5, just after the first post-NBI sawtooth crash. The results are averaged in λ with $\Delta\lambda$ = 0.2. Three cases are compared: a) the fast-ion sawtooth mixing and the ripple losses are assumed to be negligible; b) the usual fast ion mixing model is used; and c) the usual fast ion mixing and ripple models are used.

Fig. 14 Broadening of the alpha distribution, averaged over λ in the center assuming fast ion sawtooth mixing and usual ripple losses.

Central T_e and Sawteeth
Typical Evolution in Supershots

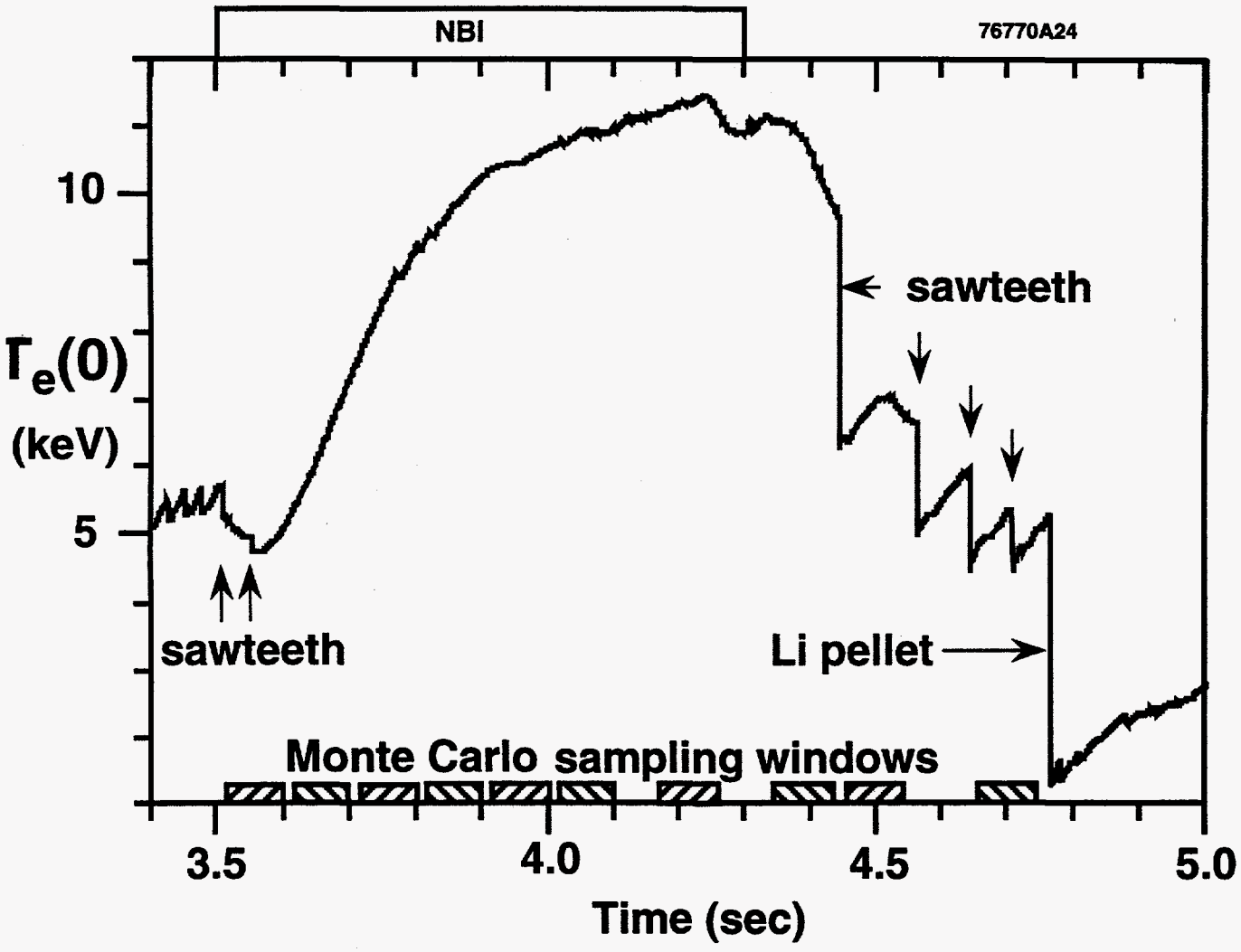

Fig. 1

Neutron Emission Components
DT Supershot

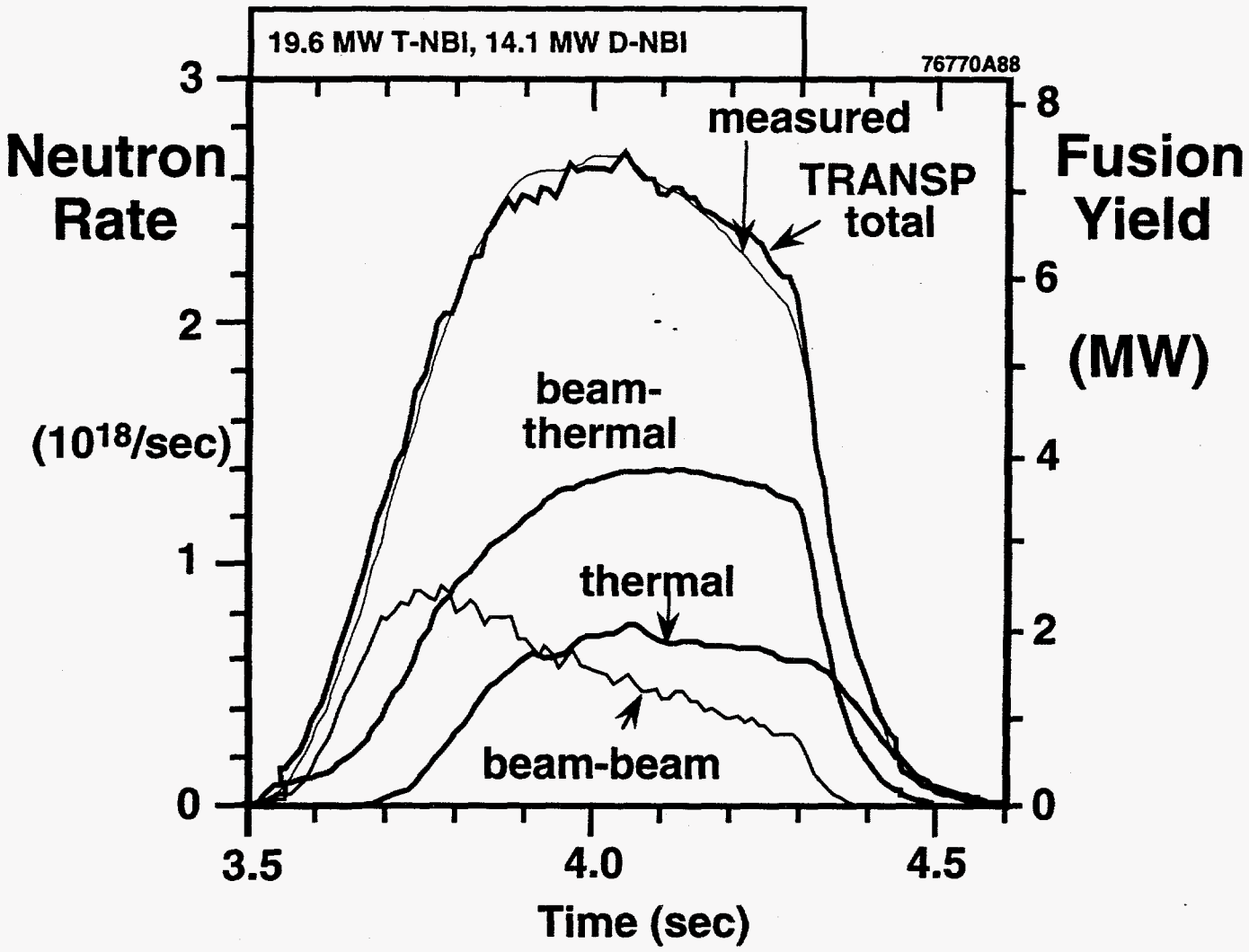

Fig. 2(a)

Neutron Chordal Emission
Comparison with measurements

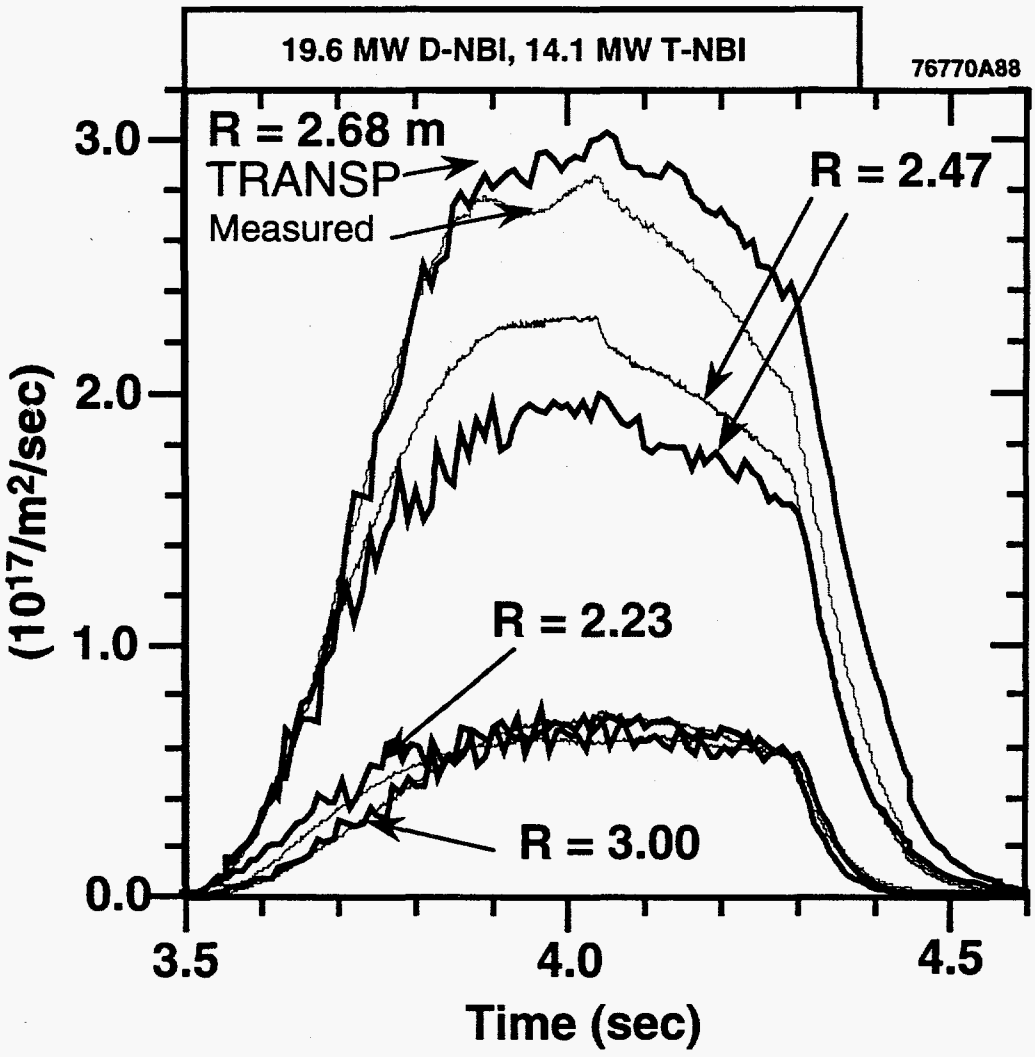

Fig. 2(b)

Chordal DT neutron emission profiles

DT-NBI supershot

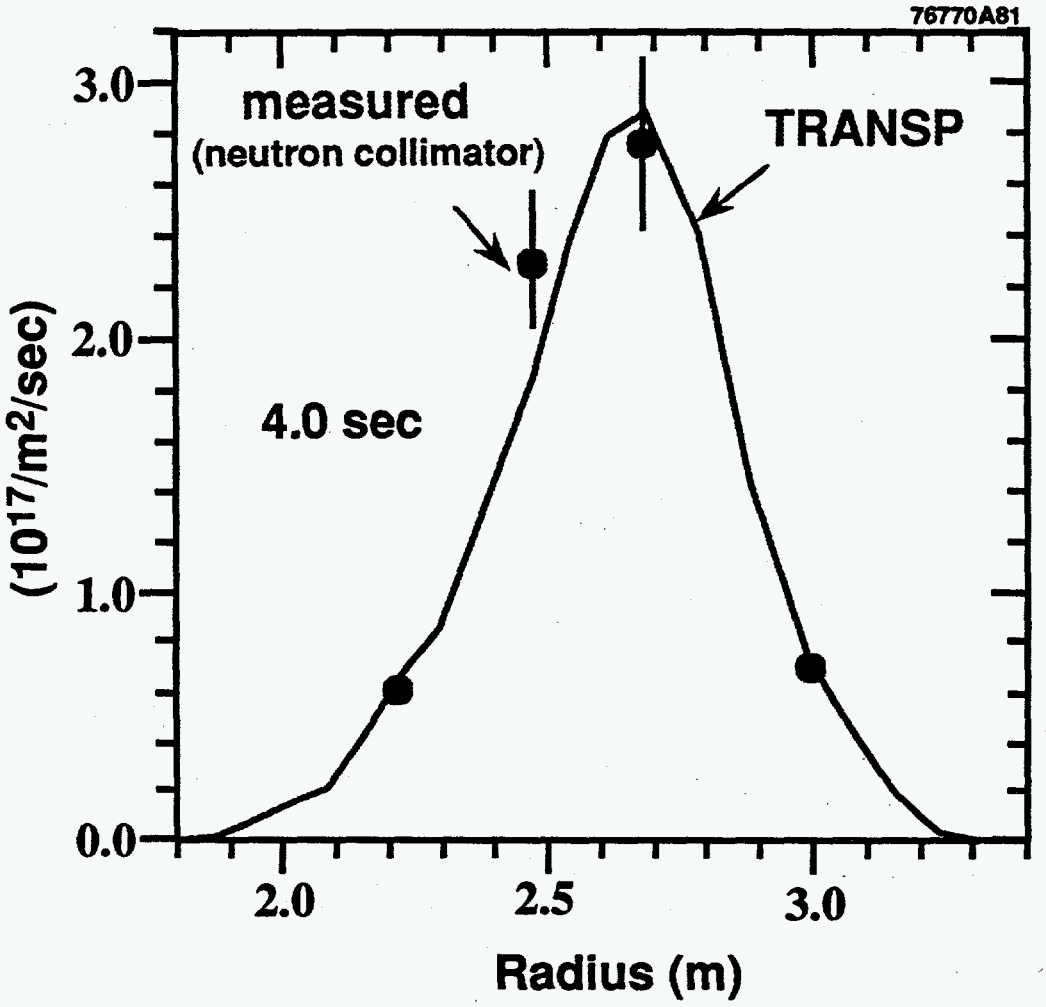

Fig. 2(c)

Central Fusion Power
Assuming no fast ion mixing

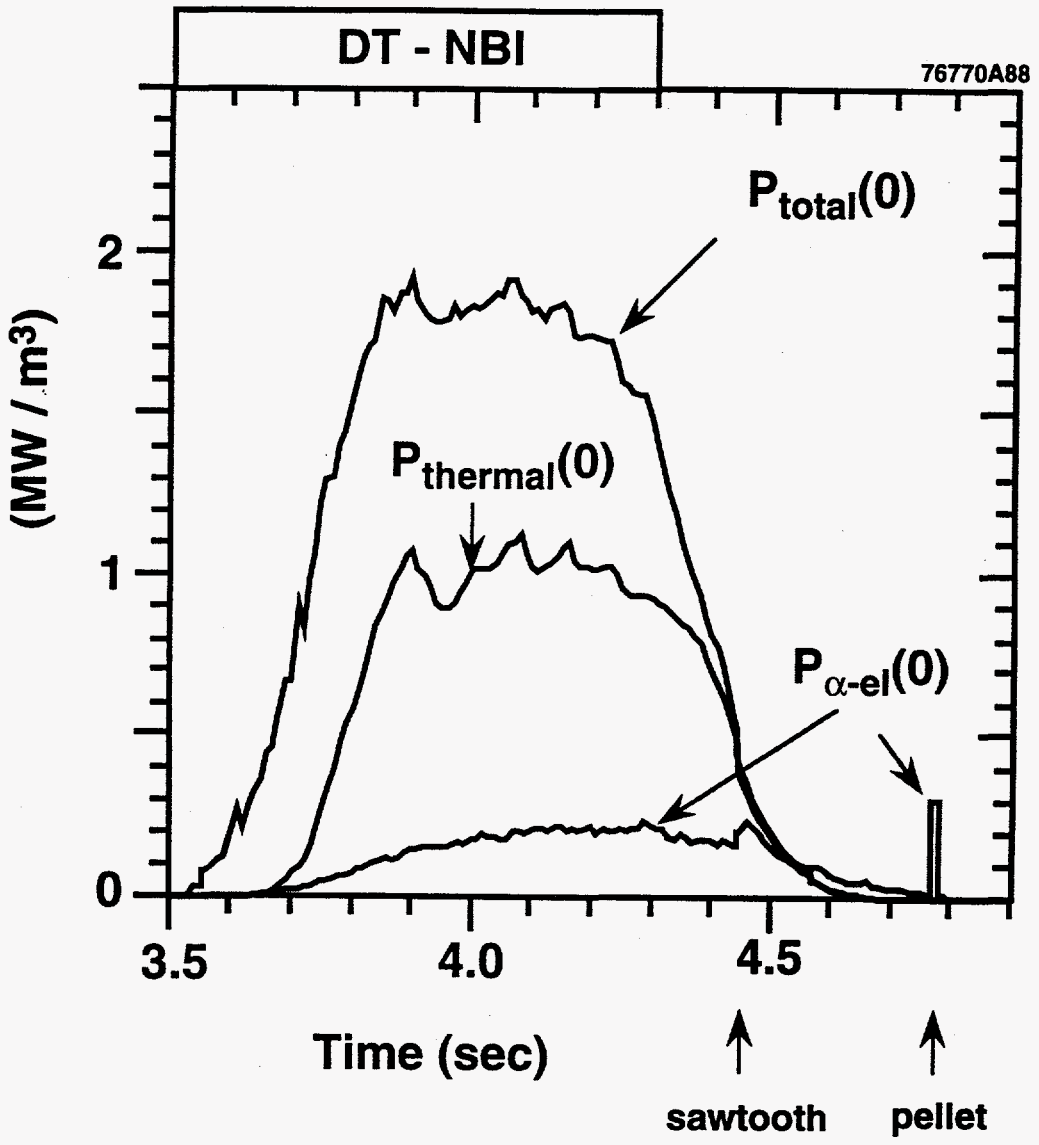

Fig. 3

Profiles of fast ion slowing down times

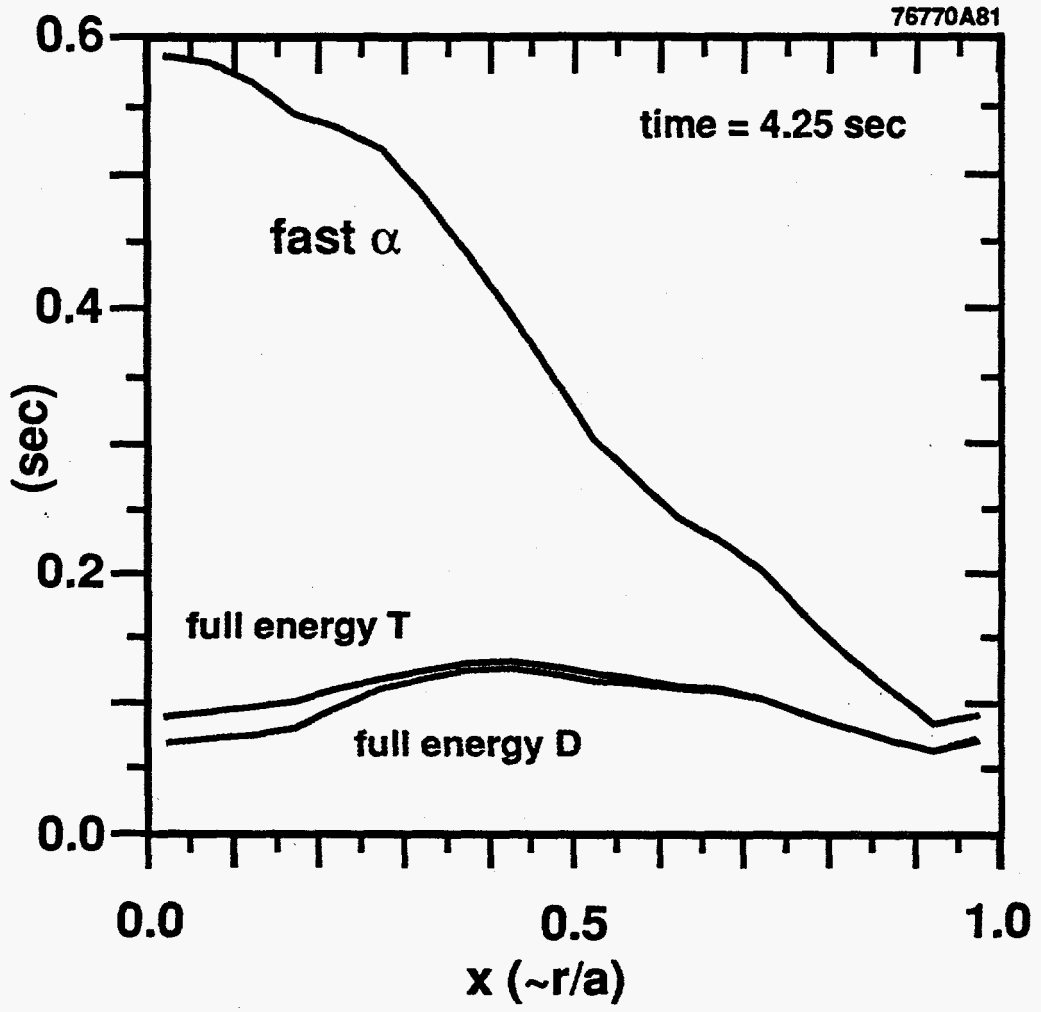

Fig. 4(a)

Profiles of fast ion pitch angle scattering times

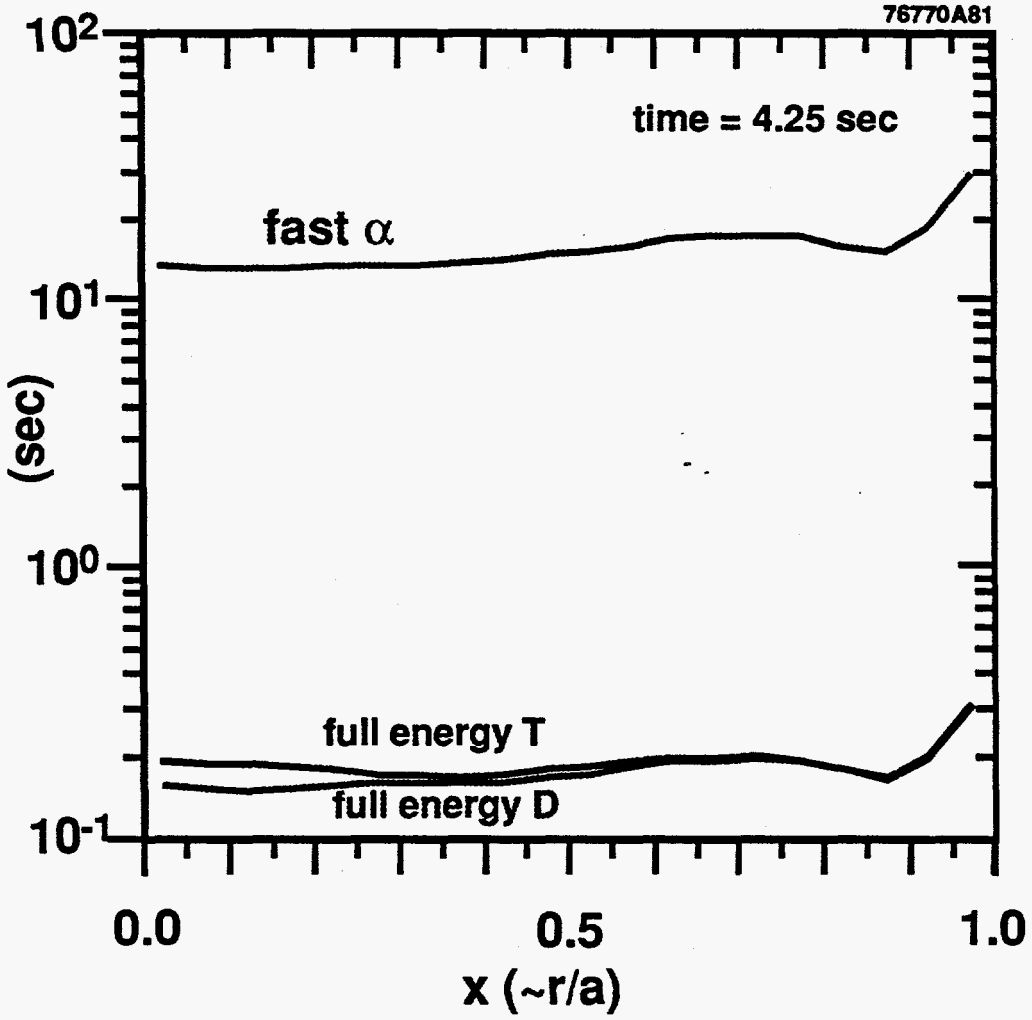

Fig. 4(b)

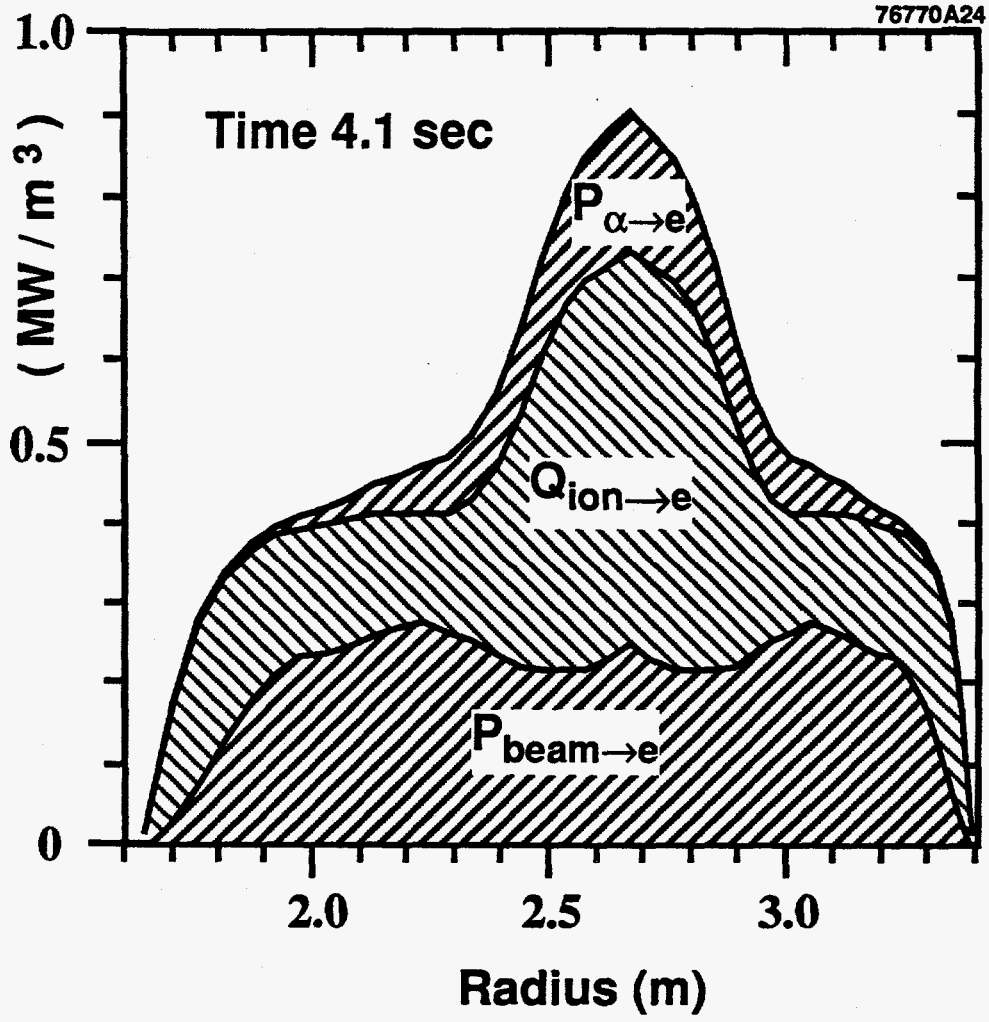
Electron heating profiles
76770A24
1.0
0.5
0
(MW / m 3)
Time 4.1 sec
P α→e
Q ion→e
P beam→e
2.0
2.5
3.0
Radius (m)

Fig. 5

Central alpha parameters
With ripple, fast ion mixing

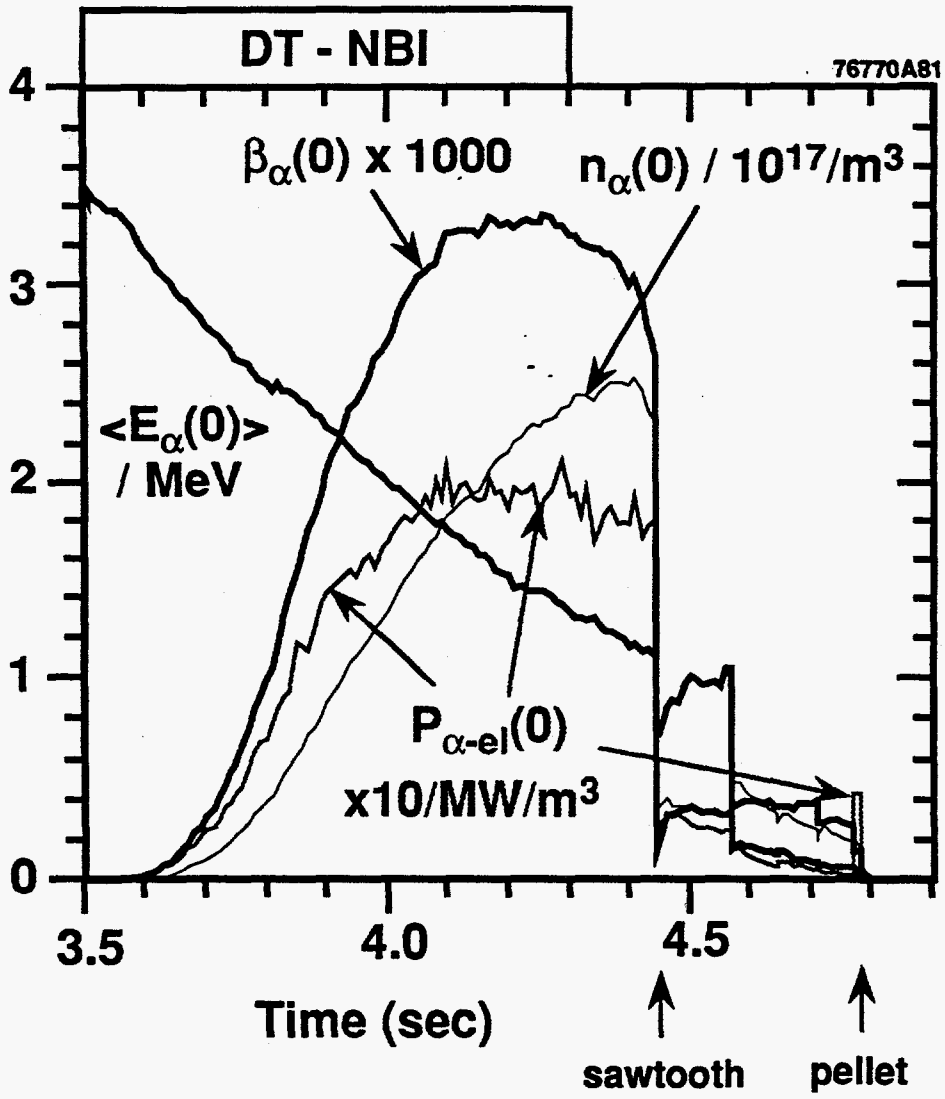

Fig. 6(a)

Central alpha parameters

With ripple, no fast ion mixing

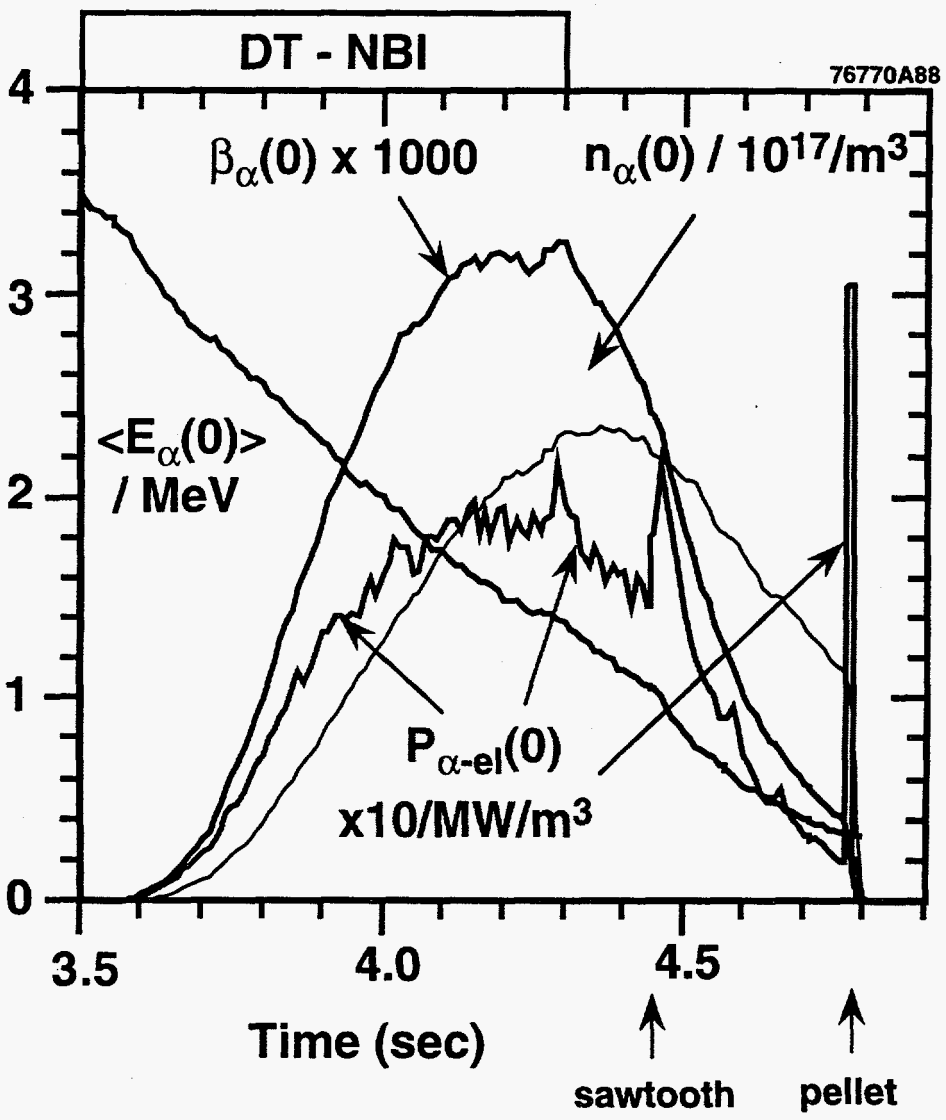

Fig. 6(b)

n_α and q_ψ profiles

After sawtooth crash

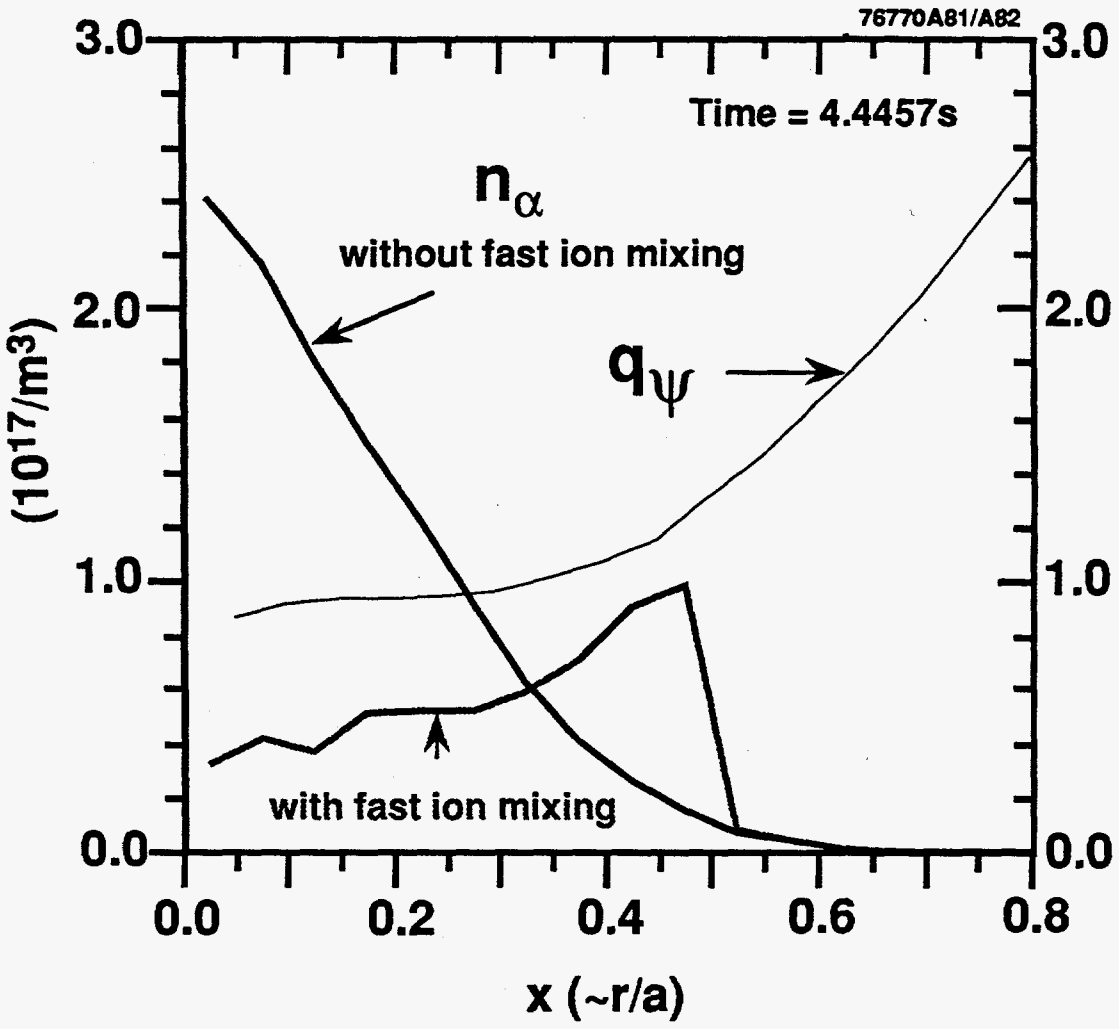

Fig. 7

n_α profiles
End of NBI

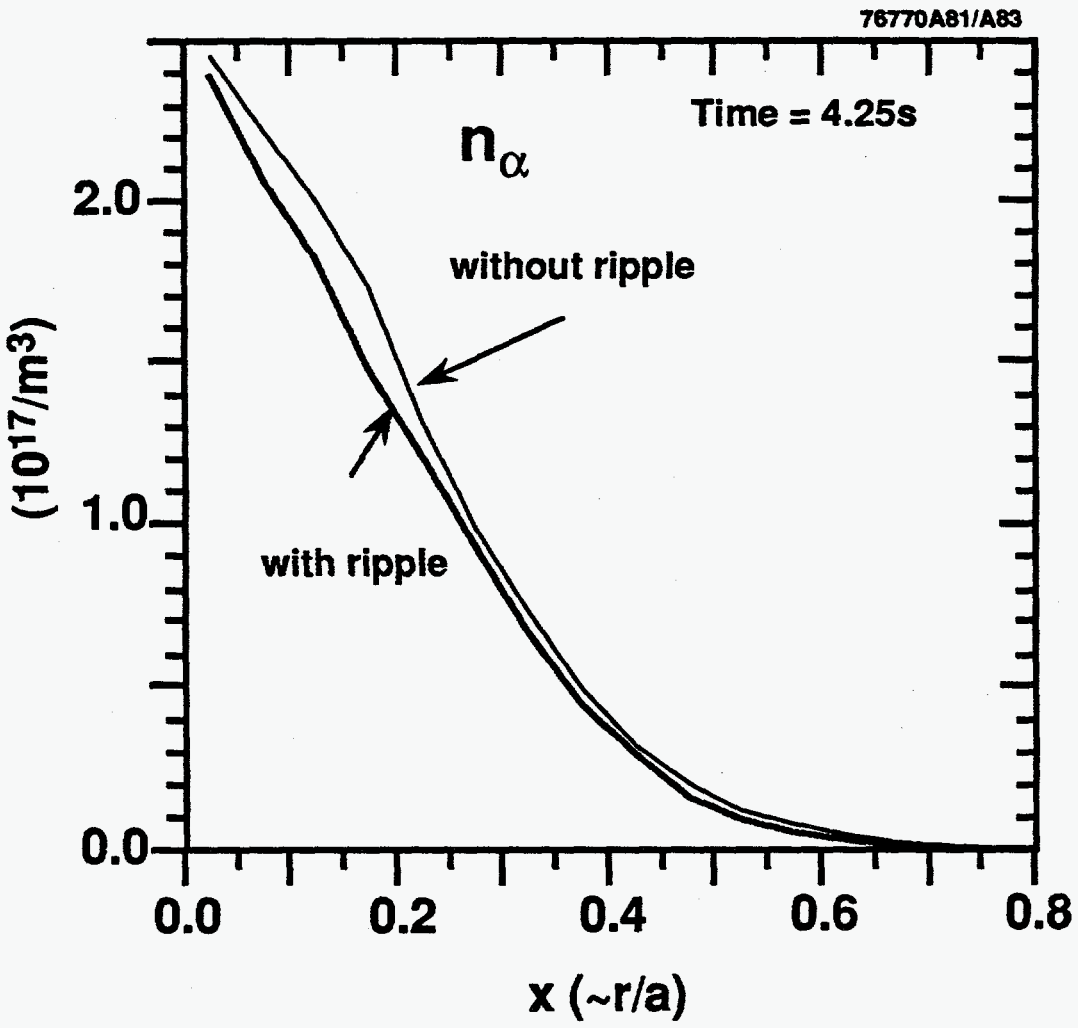

Fig. 8(a)

β_α profiles
End of NBI

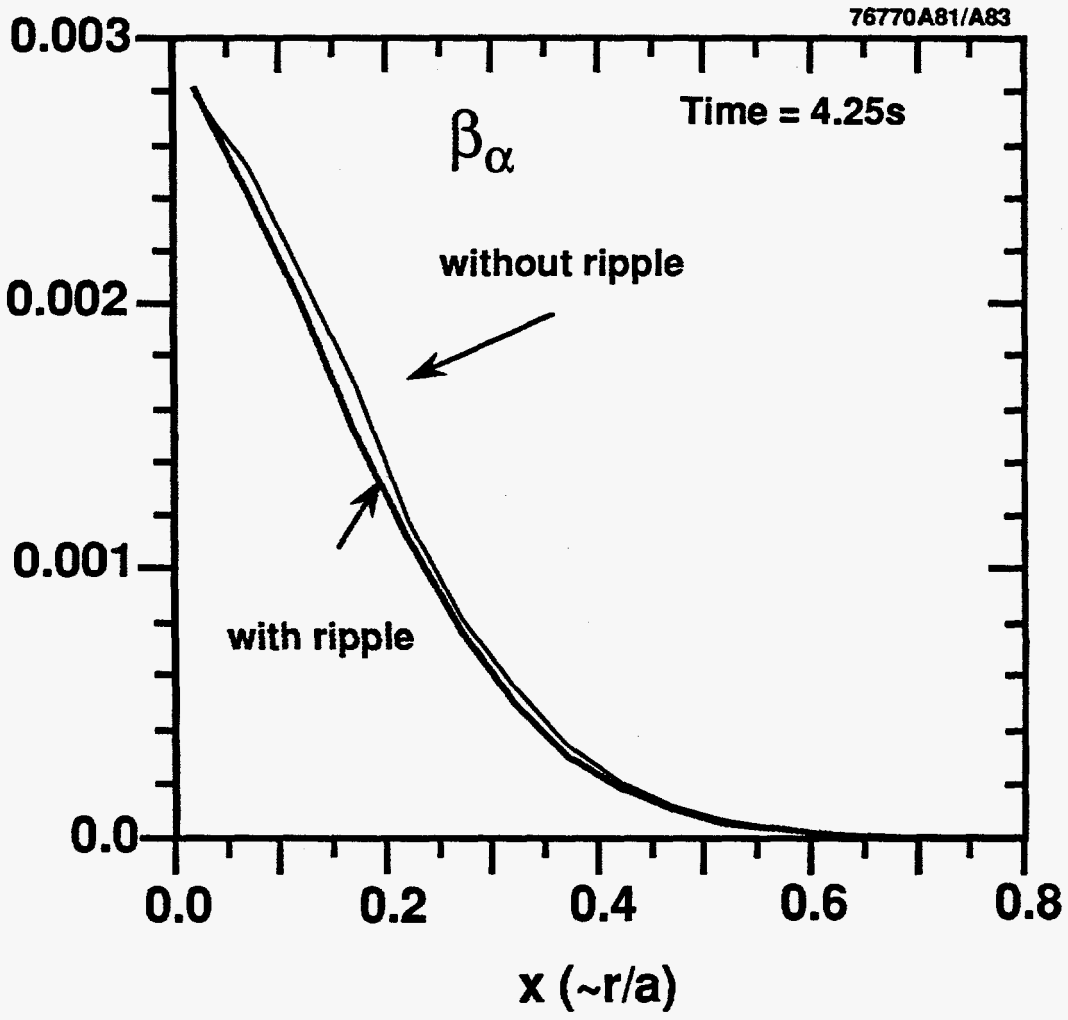

Fig. 8(b)

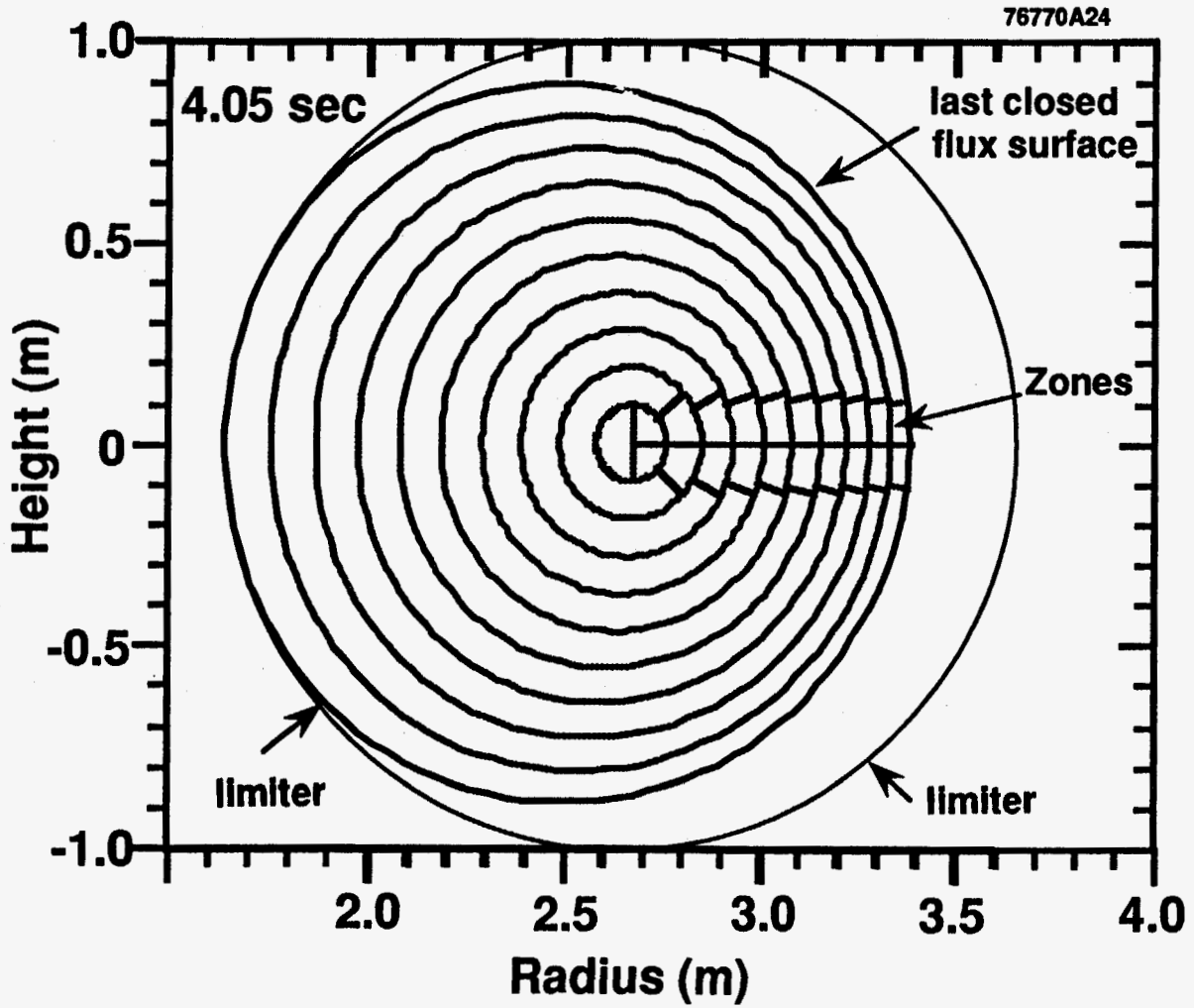
Magnetic Flux surfaces
and zones for sampling distributions
76770A24
4.05 sec
last closed
flux surface
Zones
limiter
limiter
1.0
0.5
0
-0.5
-1.0
Height (m)
2.0
2.5
3.0
3.5
4.0
Radius (m)

Fig. 9

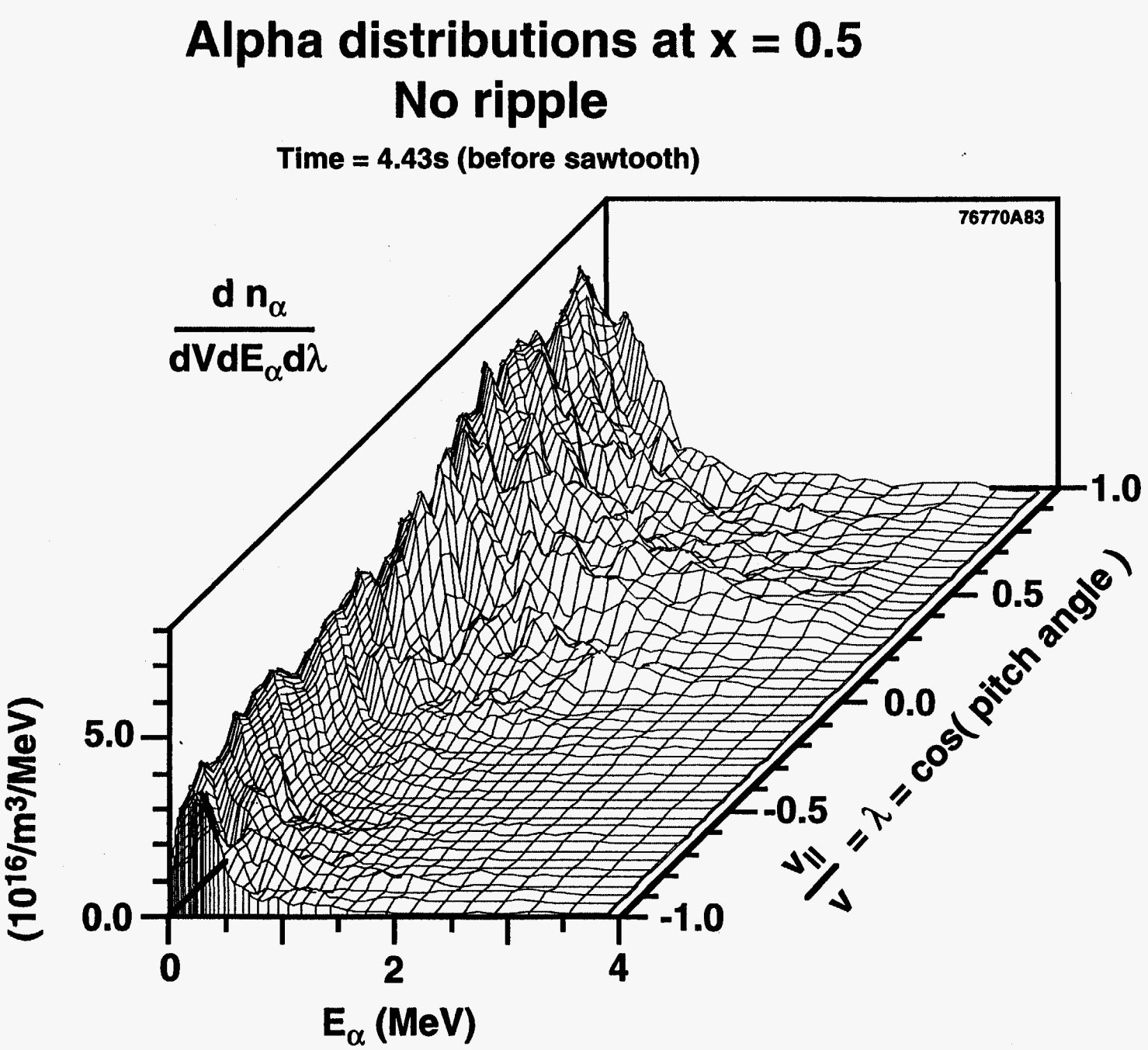
Alpha distributions at x = 0.5
No ripple
Time = 4.43s (before sawtooth)
76770A83
d n$_\alpha$ / dVdE$_\alpha$dλ
(10^{16}/m^3/MeV)
5.0
0.0
0
2
4
E$_\alpha$ (MeV)
1.0
0.5
0.0
-0.5
-1.0
v$_{||}$ / v = λ = cos(pitch angle)

Fig. 10(a)

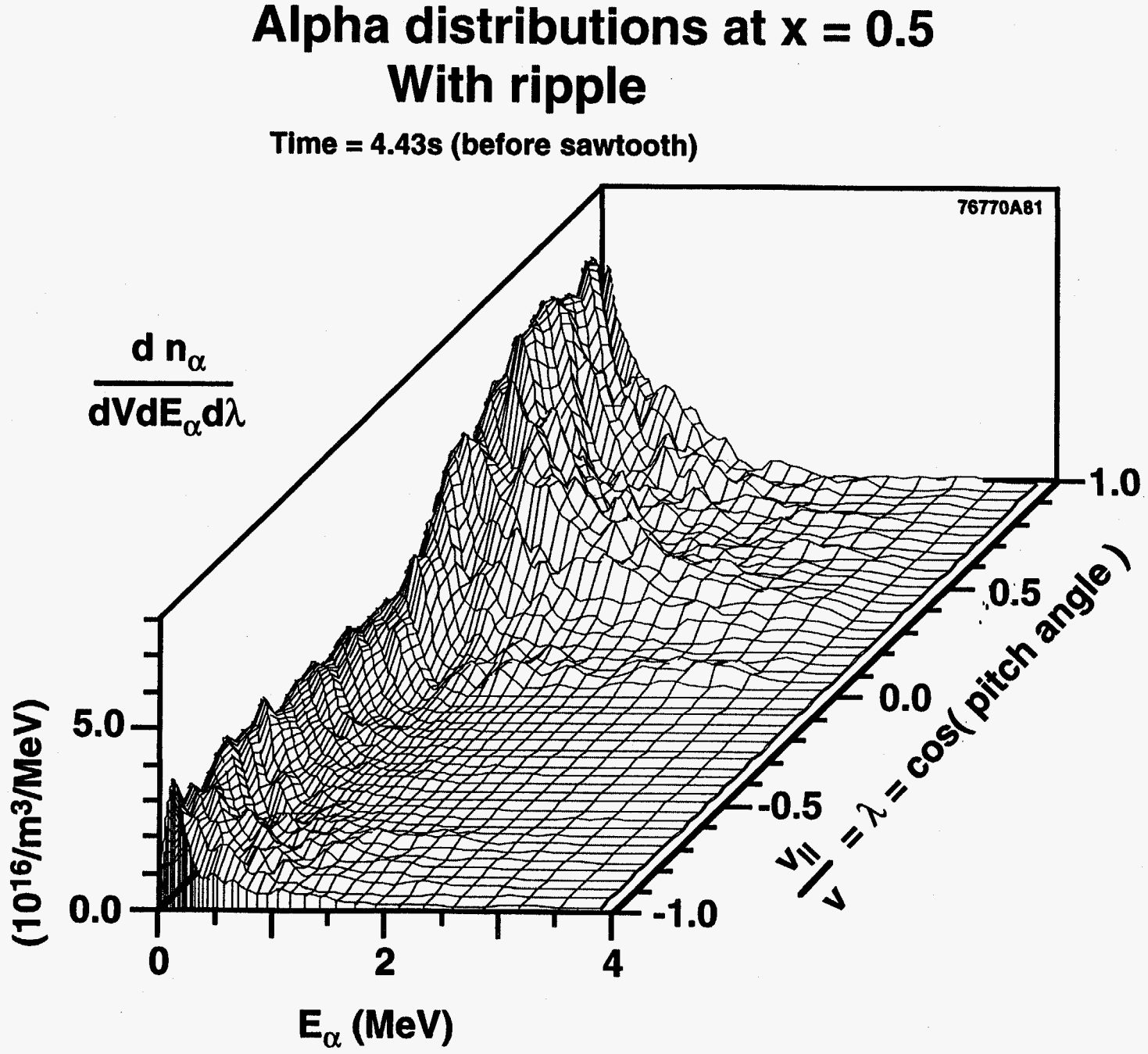
Alpha distributions at x = 0.5
With ripple
Time = 4.43s (before sawtooth)
76770A81
d n$_\alpha$
dVdE$_\alpha$dλ
(10^{16}/m^3/MeV)
5.0
0.0
0
2
4
E$_\alpha$ (MeV)
1.0
0.5
0.0
-0.5
-1.0
v$_{||}$/v = λ = cos(pitch angle)

Fig. 10(b)

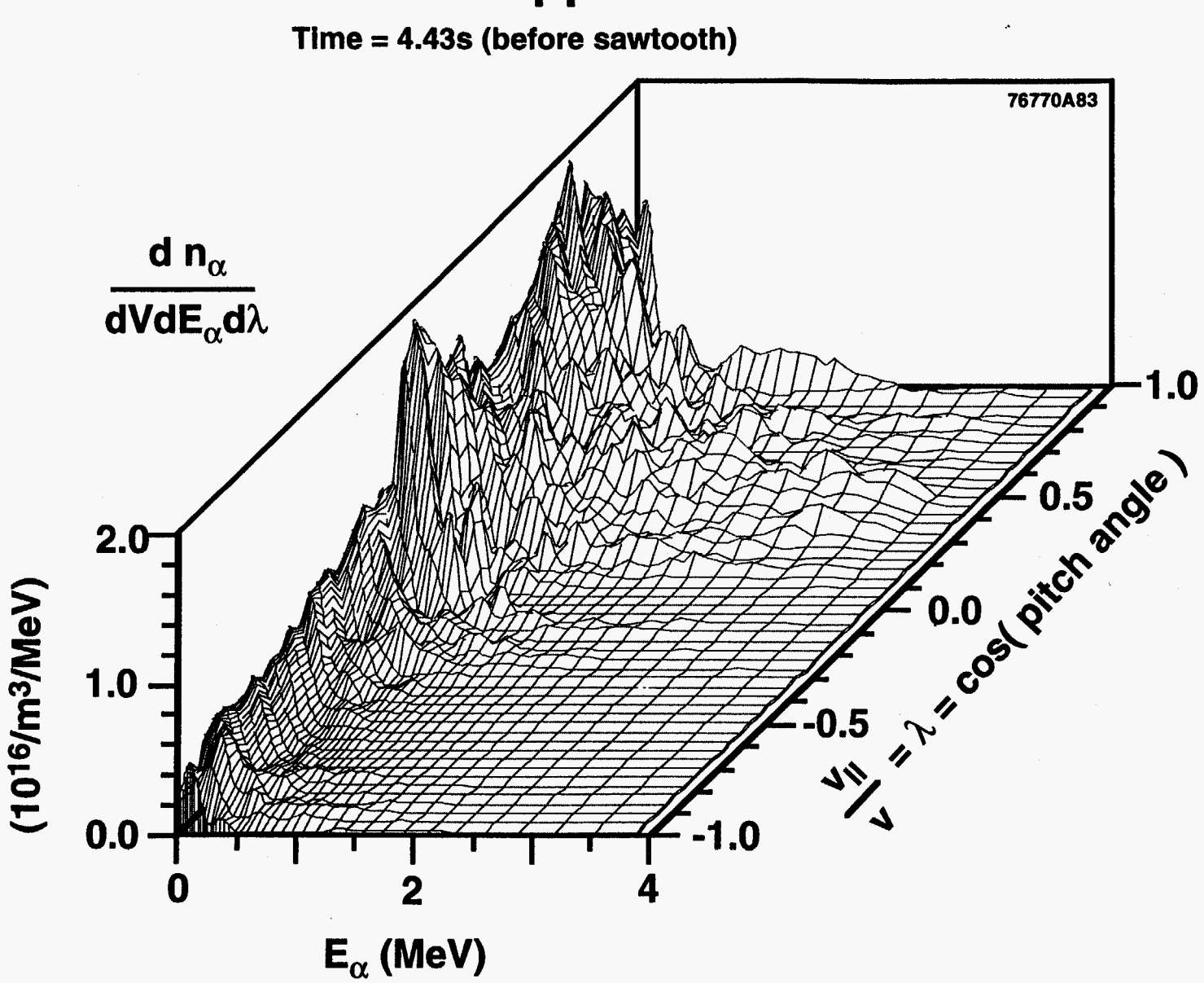
Alpha distributions at x = 0.7
No ripple
Time = 4.43s (before sawtooth)
76770A83
d n$_\alpha$ / dVdE$_\alpha$dλ
(10^{16}/m^3/MeV)
2.0
1.0
0.0
0
2
4
E$_\alpha$ (MeV)
1.0
0.5
0.0
-0.5
-1.0
v$_{||}$/v = λ = cos(pitch angle)

Fig. 11(a)

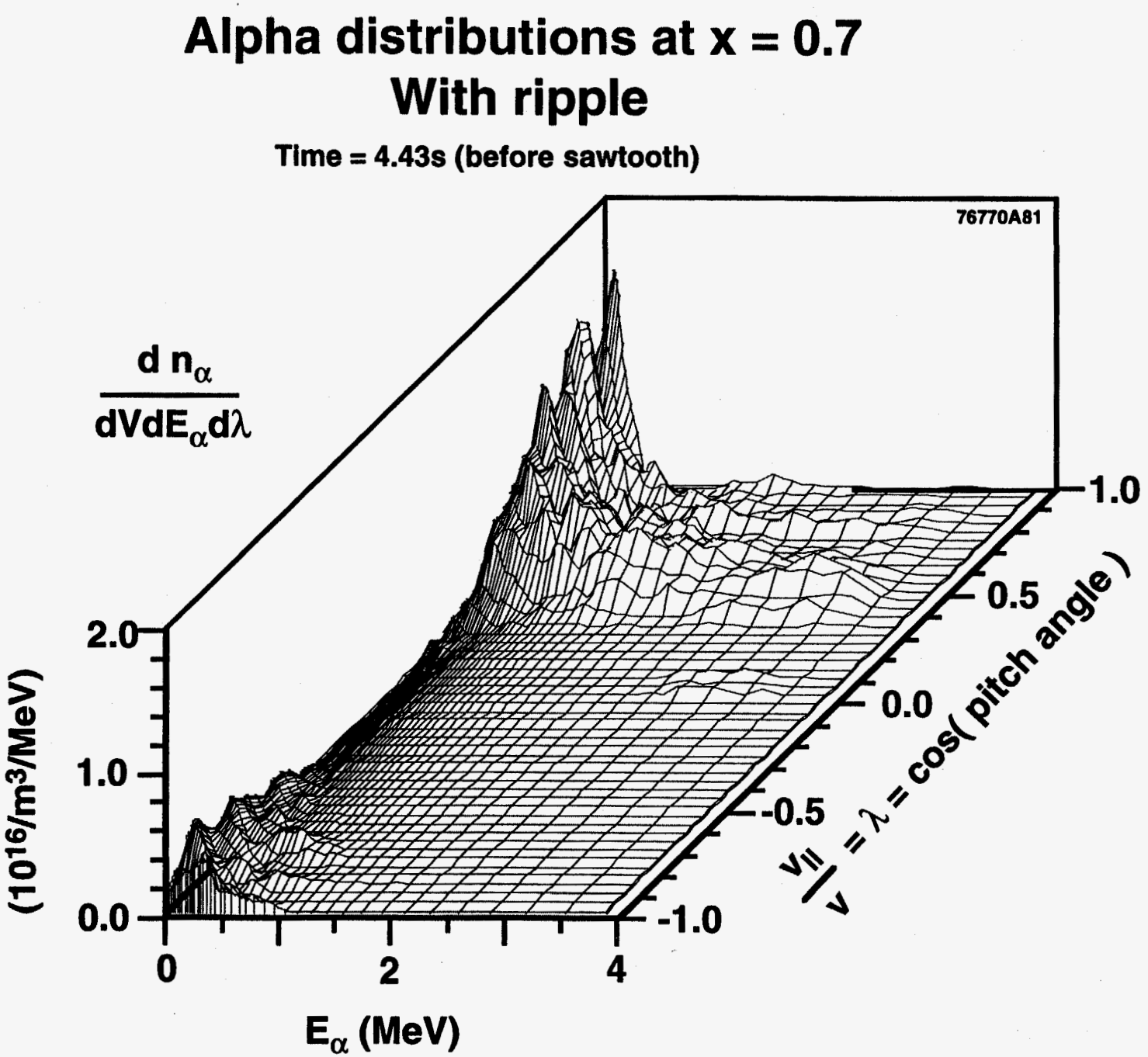
Alpha distributions at x = 0.7
With ripple
Time = 4.43s (before sawtooth)
76770A81
d n$_\alpha$
dVdE$_\alpha$dλ
(10^{16}/m^3/MeV)
2.0
1.0
0.0
0
2
4
E$_\alpha$ (MeV)
1.0
0.5
0.0
-0.5
-1.0
v$_{||}$/v = λ = cos(pitch angle)

Alpha density radial profiles

λ averaged from -0.1 to +0.1

DT- NBI 3.5 - 4.3 sec

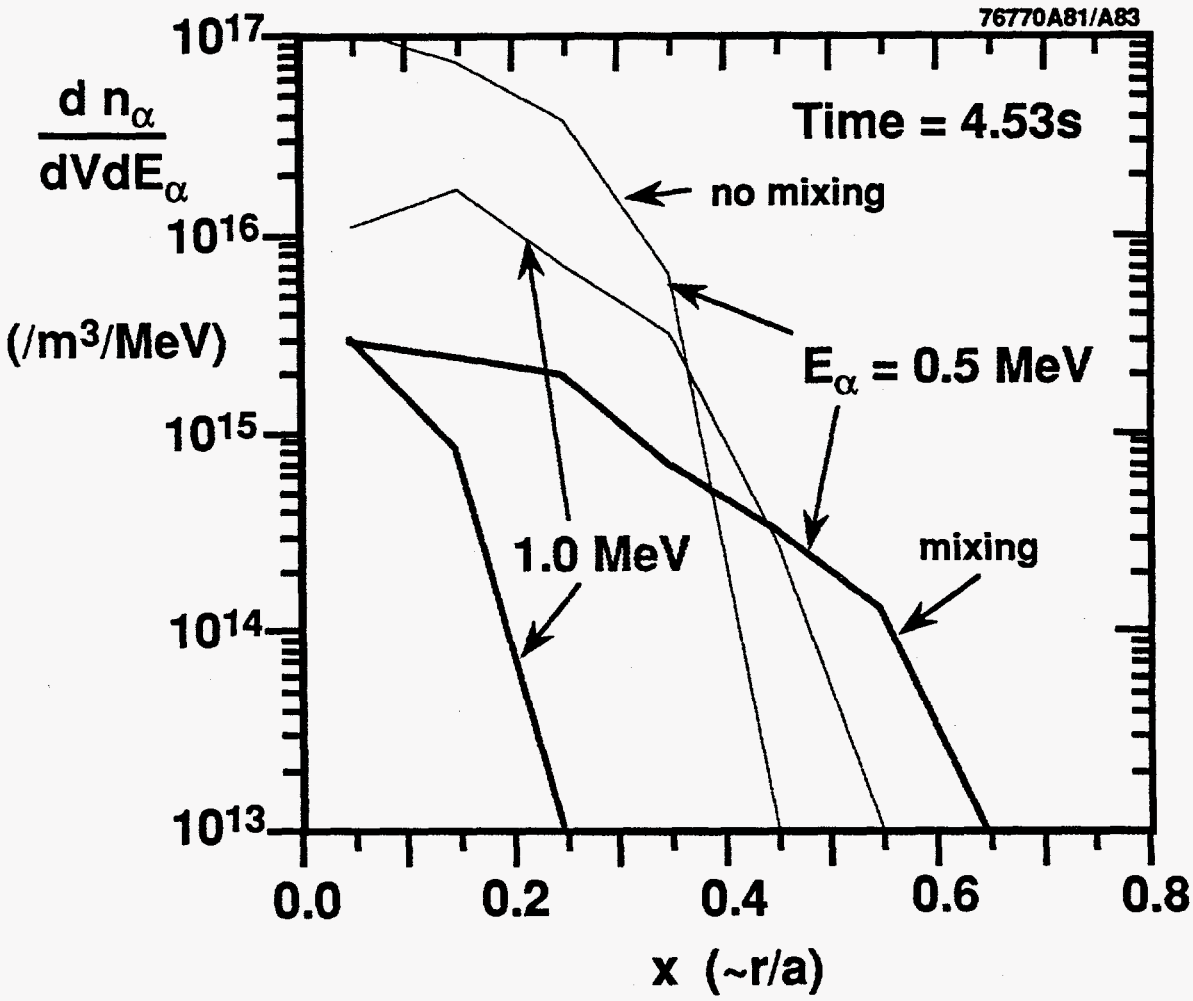

Fig. 12

Alpha pitch angle distributions
No ripple, no mixing

x = 0.5 Time = 4.53 sec

19.4 MW T-NBI, 14.0 MW D-NBI from 3.5 to 4.3 sec

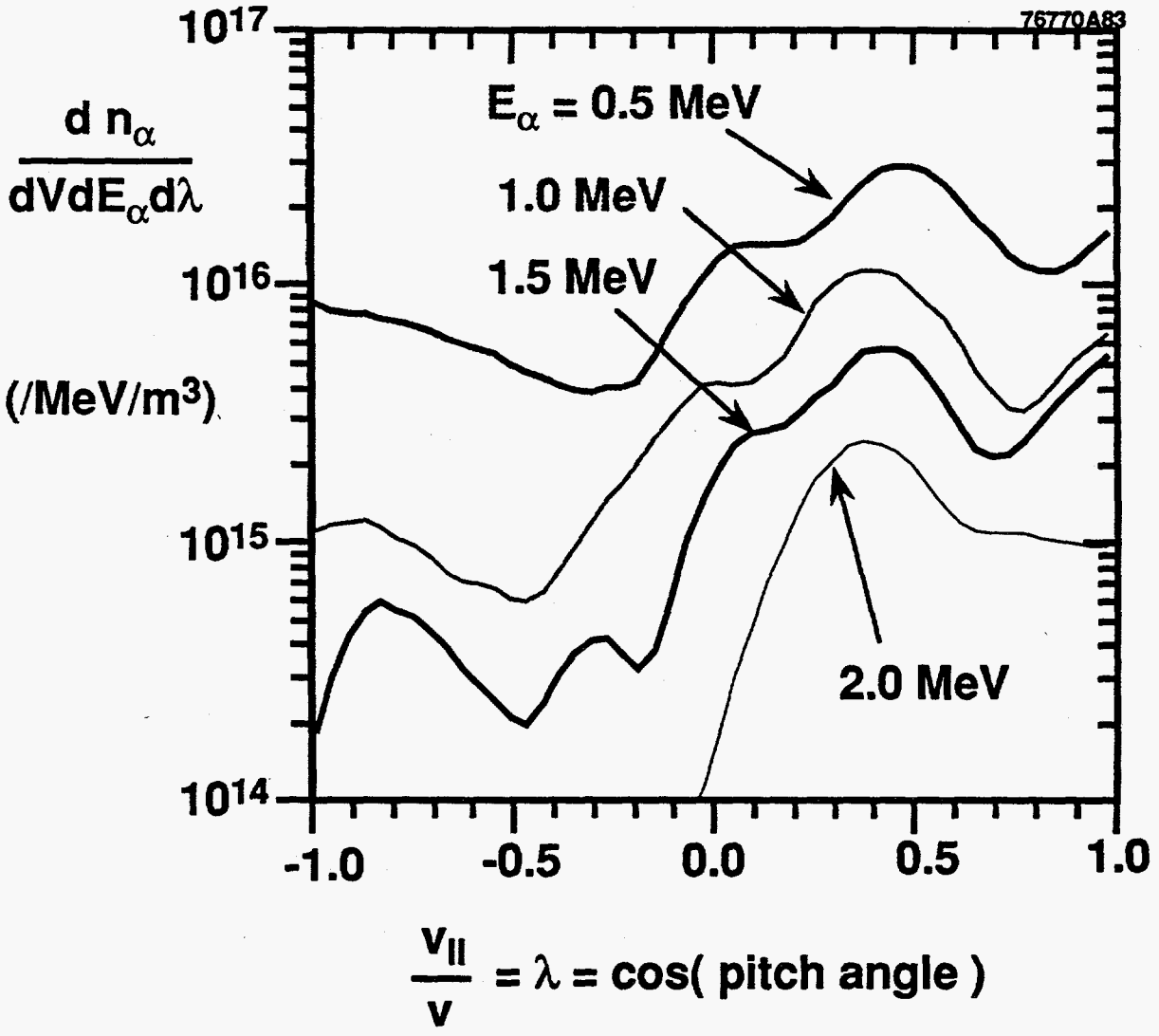

Fig. 13(a)

Alpha pitch angle distributions
No ripple, with mixing

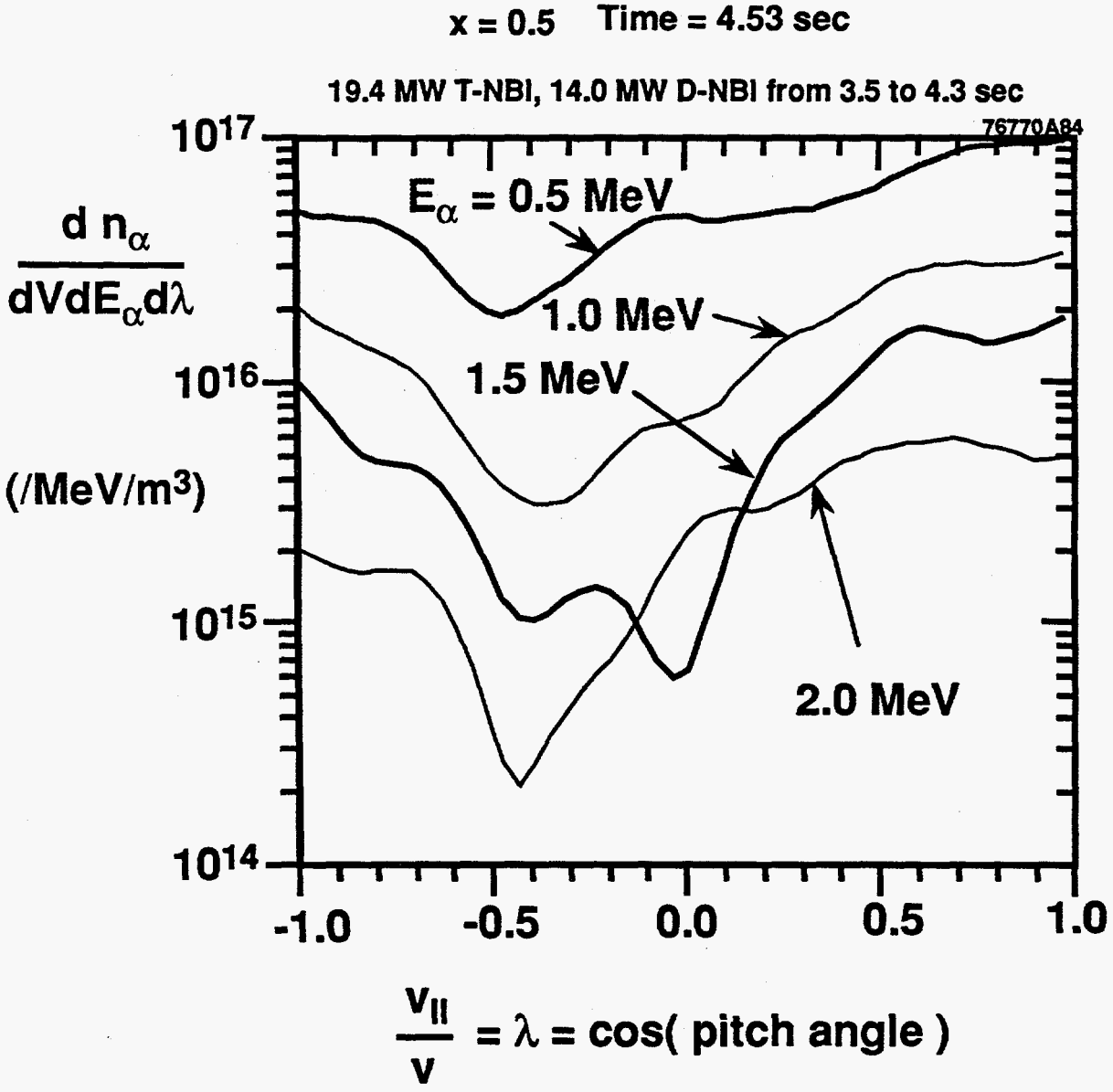

Fig. 13(b)

Alpha pitch angle distributions
With ripple and mixing

x = 0.5 Time = 4.53 sec

19.4 MW T-NBI, 14.0 MW D-NBI from 3.5 to 4.3 sec

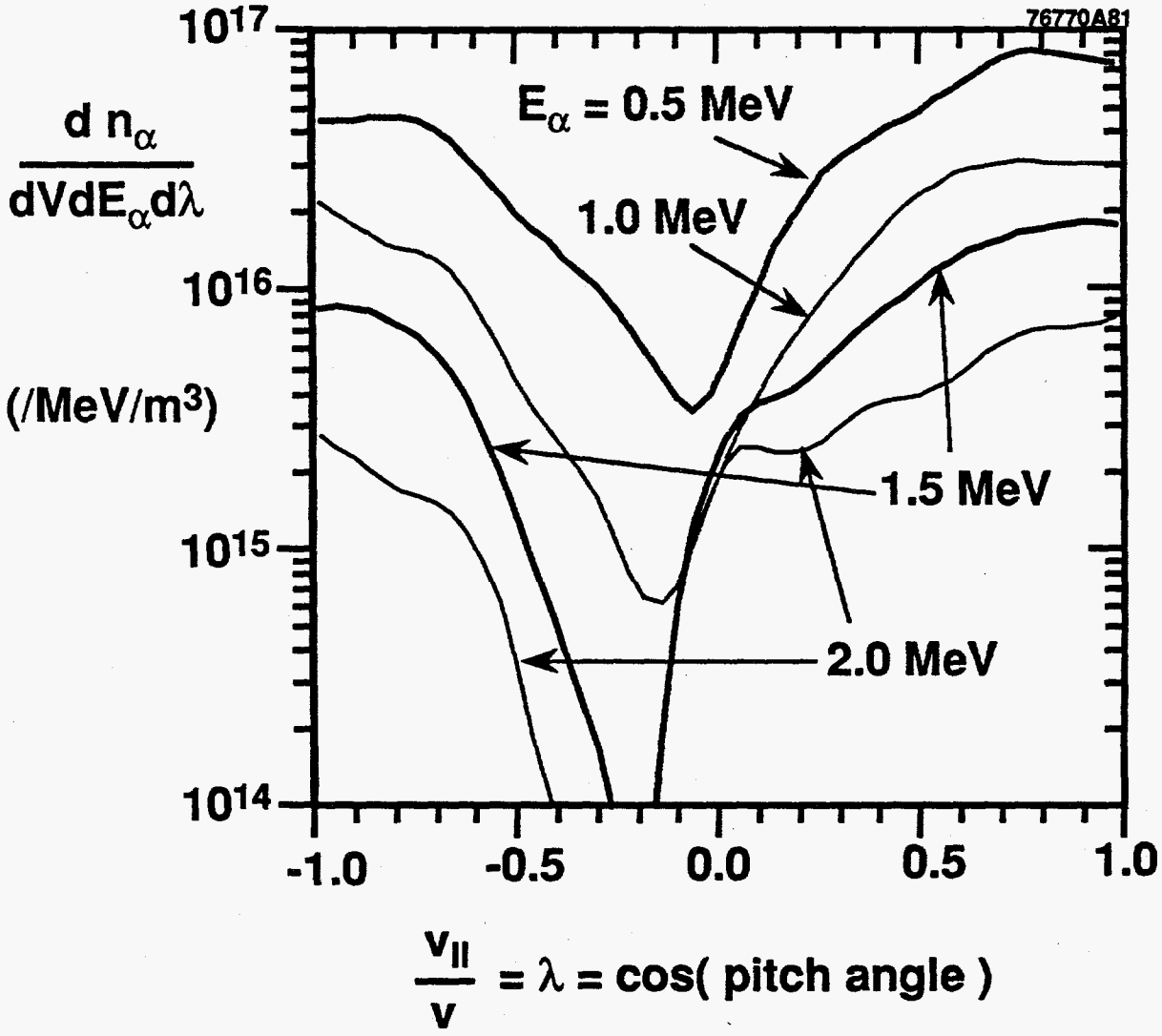

Fig. 13(c)

Central alpha energy distributions

DT Supershot with Fusion Yield = 7.5 MW

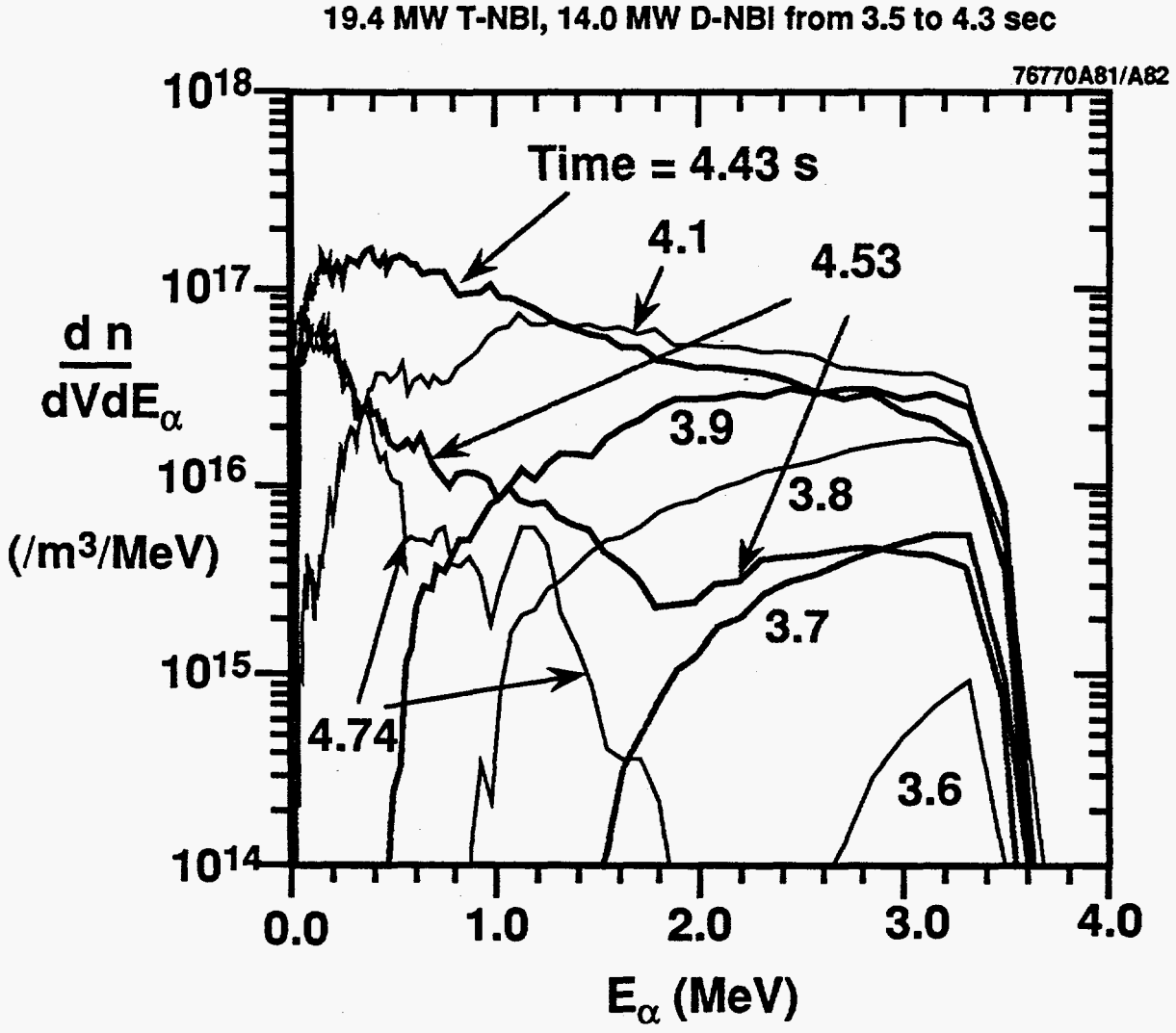

Fig. 14

EXTERNAL DISTRIBUTION IN ADDITION TO UC-420

Dr. F. Paoloni, Univ. of Wollongong, AUSTRALIA
Prof. R.C. Cross, Univ. of Sydney, AUSTRALIA
Plasma Research Lab., Australian Nat. Univ., AUSTRALIA
Prof. I.R. Jones, Flinders Univ, AUSTRALIA
Prof. F. Cap, Inst. for Theoretical Physics, AUSTRIA
Prof. M. Heindler, Institut für Theoretische Physik, AUSTRIA
Prof. M. Goossens, Astronomisch Instituut, BELGIUM
Ecole Royale Militaire, Lab. de Phy. Plasmas, BELGIUM
Commission-European, DG. XII-Fusion Prog., BELGIUM
Prof. R. Boucique, Rijksuniversiteit Gent, BELGIUM
Dr. P.H. Sakanaka, Instituto Fisica, BRAZIL
Prof. Dr. I.C. Nascimento, Instituto Fisica, Sao Paulo, BRAZIL
Instituto Nacional De Pesquisas Espaciais-INPE, BRAZIL
Documents Office, Atomic Energy of Canada Ltd., CANADA
Ms. M. Morin, CCFM/Tokamak de Varennes, CANADA
Dr. M.P. Bachynski, MPB Technologies, Inc., CANADA
Dr. H.M. Skarsgard, Univ. of Saskatchewan, CANADA
Prof. J. Teichmann, Univ. of Montreal, CANADA
Prof. S.R. Sreenivasan, Univ. of Calgary, CANADA
Prof. R. Marchand, INRS-Energie et Materiaux, CANADA
Dr. R. Bolton, Centre canadien de fusion magnétique, CANADA
Dr. C.R. James,, Univ. of Alberta, CANADA
Dr. P. Lukác, Komenského Universzita, CZECHO-SLOVAKIA
The Librarian, Culham Laboratory, ENGLAND
Library, R61, Rutherford Appleton Laboratory, ENGLAND
Mrs. S.A. Hutchinson, JET Library, ENGLAND
Dr. S.C. Sharma, Univ. of South Pacific, FIJI ISLANDS
P. Mähönen, Univ. of Helsinki, FINLAND
Prof. M.N. Bussac, Ecole Polytechnique,, FRANCE
C. Mouttet, Lab. de Physique des Milieux Ionisés, FRANCE
J. Radet, CEN/CADARACHE - Bat 506, FRANCE
Prof. E. Economou, Univ. of Crete, GREECE
Ms. C. Rinni, Univ. of Ioannina, GREECE
Preprint Library, Hungarian Academy of Sci., HUNGARY
Dr. B. DasGupta, Saha Inst. of Nuclear Physics, INDIA
Dr. P. Kaw, Inst. for Plasma Research, INDIA
Dr. P. Rosenau, Israel Inst. of Technology, ISRAEL
Librarian, International Center for Theo Physics, ITALY
Miss C. De Palo, Associazione EURATOM-ENEA , ITALY
Dr. G. Grosso, Istituto di Fisica del Plasma, ITALY
Prof. G. Rostangni, Istituto Gas Ionizzati Del Cnr, ITALY
Dr. H. Yamato, Toshiba Res & Devel Center, JAPAN
Prof. I. Kawakami, Hiroshima Univ., JAPAN
Prof. K. Nishikawa, Hiroshima Univ., JAPAN
Librarian, Naka Fusion Research Establishment, JAERI, JAPAN
Director, Japan Atomic Energy Research Inst., JAPAN
Prof. S. Itoh, Kyushu Univ., JAPAN
Research Info. Ctr., National Instit. for Fusion Science, JAPAN
Prof. S. Tanaka, Kyoto Univ., JAPAN
Library, Kyoto Univ., JAPAN
Prof. N. Inoue, Univ. of Tokyo, JAPAN
Secretary, Plasma Section, Electrotechnical Lab., JAPAN
Dr. O. Mitarai, Kumamoto Inst. of Technology, JAPAN
Dr. G.S. Lee, Korea Basic Sci. Ctr., KOREA
J. Hyeon-Sook, Korea Atomic Energy Research Inst., KOREA
D.I. Choi, The Korea Adv. Inst. of Sci. & Tech., KOREA
Leandro Melendez Lugo, Inst. Nac'l. de Inves. Nucl, MEXICO
Prof. B.S. Liley, Univ. of Waikato, NEW ZEALAND
Inst of Physics, Chinese Acad Sci PEOPLE'S REP. OF CHINA
Library, Inst. of Plasma Physics, PEOPLE'S REP. OF CHINA
Tsinghua Univ. Library, PEOPLE'S REPUBLIC OF CHINA
Z. Li, S.W. Inst Physics, PEOPLE'S REPUBLIC OF CHINA
Prof. J.A.C. Cabral, Instituto Superior Tecnico, PORTUGAL
Prof. M.A. Hellberg, Univ. of Natal, S. AFRICA
Prof. D.E. Kim, Pohang Inst. of Sci. & Tech., SO. KOREA
Prof. C.I.E.M.A.T, Fusion Division Library, SPAIN
Dr. L. Stenflo, Univ. of UMEA, SWEDEN
Library, Royal Inst. of Technology, SWEDEN
Prof. H. Wilhelmson, Chalmers Univ. of Tech., SWEDEN
Centre Phys. Des Plasmas, Ecole Polytech, SWITZERLAND
Bibliotheek, Inst. Voor Plasma-Fysica, THE NETHERLANDS
Asst. Prof. Dr. S. Cakir, Middle East Tech. Univ., TURKEY
Dr. V.A. Glukhikh,Sci. Res. Inst. Electrophys.I Apparatus, USSR
Dr. D.D. Ryutov, Siberian Branch of Academy of Sci., USSR
Dr. G.A. Eliseev, I.V. Kurchatov Inst., USSR
Librarian, The Ukr.SSR Academy of Sciences, USSR
Dr. L.M. Kovrizhnykh, Inst. of General Physics, USSR
Kernforschungsanlage GmbH, Zentralbibliothek, W. GERMANY
Bibliothek, Inst. Für Plasmaforschung, W. GERMANY
Prof. K. Schindler, Ruhr-Universität Bochum, W. GERMANY
Dr. F. Wagner, (ASDEX), Max-Planck-Institut, W. GERMANY
Librarian, Max-Planck-Institut, W. GERMANY